

# Robust Quantum Control: Analysis & Synthesis via Averaging

Robert L. Kosut,<sup>1,2</sup> Gaurav Bhole,<sup>2</sup> and Herschel Rabitz<sup>2</sup>

<sup>1</sup>*SC Solutions, Sunnyvale CA, 94085*

<sup>2</sup>*Department of Chemistry, Princeton University, Princeton, NJ, 08544*

(Dated: August 31, 2022)

An approach is presented for robustness analysis and quantum (unitary) control synthesis based on the classic method of averaging. The result is a multicriterion optimization competing the nominal (uncertainty-free) fidelity with a well known robustness measure: the size of an interaction (error) Hamiltonian, essentially the first term in the Magnus expansion of an interaction unitary. Combining this with the fact that the topology of the control landscape at high fidelity is determined by the null space of the nominal fidelity Hessian, we arrive at a new two-stage algorithm. Once the nominal fidelity is sufficiently high, we approximate both the nominal fidelity and robustness measure as quadratics in the control increments. An optimal solution is obtained by solving a convex optimization for the control increments at each iteration to keep the nominal fidelity high and reduce the robustness measure. Additionally, by separating fidelity from the robustness measure, more flexibility is available for uncertainty modeling.

## I. INTRODUCTION

For a quantum computer that is *ideally* composed of a temporal sequence of unitary logic gates, robustness means that at specified times, despite imperfections or perturbations, each *actual* gate operation is sufficiently close to its ideal for the intended purpose, *i.e.*, errors are all below a threshold value which allows for a quantum computation.

In this paper, the standard state transformation used in the *method of averaging* [1] is modified for quantum systems resulting in a robustness framework useful for both analysis and control synthesis. In particular, what arises from the theory is a *multicriterion control objective*: maximize the fidelity corresponding to the control dependent nominal (perturbation-free) unitary *and* minimize a term (or terms) dependent on the characteristics of the uncertainty model. Specifically, robustness is measured by the size of the first term in the Magnus expansion of a unitary evolving from a Hamiltonian dependent on the interaction of the nominal unitary and the Hamiltonian uncertainty. Suppressing this term is an underlying condition in the theoretical foundations of both dynamical decoupling [2–7] and optimization methods for general noise suppression using filter functions [8–16]. In a similar way, averaging theory establishes that if this term is made sufficiently small, and the nominal fidelity is maximized, then the effect of uncertain errors, which need not necessarily be small, can be significantly alleviated.

In the approach presented here, the inherent multicriterion control objective is intentionally maintained because of a special quantum control landscape property: when the nominal fidelity is near its maximum and the gradient is near zero, a large null space remains specified by the Hessian [17–22]. This freedom, which serves as a space to project the system disturbances, also motivates a new two-stage algorithm. First, only the nominal fidelity is maximized until a high fidelity threshold is crossed. Then the optimization minimizes the robustness measure while keeping the nominal fidelity above the threshold. The uncertainty-free optimization in the first stage, assuming sufficient control resources, can be accomplished by any iterative ascent method. For the second stage,

we show that by approximating both the nominal fidelity and the robustness measure as quadratic functions in the control increments (via gradients and Hessians), a robust control can be found by solving a convex optimization problem at each iteration.

A second consequence of separating the robustness measure from the nominal fidelity is that additional flexibility is provided for *uncertainty modeling*, *i.e.*, incorporating more specific characteristics of error sources in the robustness measure. For example, some of the errors delineated here seem naturally accounted for by time-domain uncertainty modeling. When the uncertainty, or perturbation, can also be represented by a power spectral density, or has distinct spectral lines, then the associated time-domain robustness measure can be expressed equivalently in the frequency domain using filter functions in a manner similar to that in [8–16].

The paper is organized as follows: §II describes the basic quantum system, §III presents the averaging theory, §IV describes the multicriterion optimization problem and the two-stage algorithm, §V delineates some common uncertainty models and associated interaction representations (summarized in Table I), §VI provides selected representative numerical examples, and §VII makes a few concluding remarks. Appendices contain the averaging theory proof, a detailed description of the second stage convex optimization, and some additional uncertainty models and numerical examples.

**Notation** Continuous-time functions such as a unitary are denoted by  $U(t)$  over the time interval  $t \in [0, T]$ . For discrete-time representations we use  $t$  as a time index  $t = 1 : N$  where  $U_t$  is the value of  $U(t)$  at the end of each of  $N$  uniformly spaced intervals of width  $T/N$ .  $I_n$  is the  $n \times n$  identity matrix. We use a few norms: for an  $n$ -vector  $x$ ,  $\|x\|_2$  is the two-norm, for an  $n \times m$  matrix  $X$ ,  $\|X\|_2$  is the maximum singular value of the matrix,  $\|X\|_{\text{fro}}$  is the Frobenius matrix norm (*i.e.*, the two-norm of the singular values),  $\|X\|_{\text{nuc}}$  is the nuclear norm, the sum of the singular values, and  $\|X\|_{\infty}$  is the max-row-sum. We sometimes write  $\|\cdot\|$  with no subscript, usually meaning the norm will be defined in context. For an  $n \times m$  matrix  $A$  we denote by  $\vec{A}$ , the  $nm \times 1$  vector formed by stacking the columns of  $A$  from left to right.

## II. QUANTUM SYSTEM

The quantum systems addressed are mainly focused on *closed* systems. Our framework for robust control can easily include open systems which are briefly discussed in §C8. The closed  $n$ -dimensional quantum system unitary evolution  $U(t)$  over  $t \in [0, T]$  is obtained from,

$$\begin{aligned} i\dot{U}(t) &= \left( \bar{H}(t) + \tilde{H}(t) \right) U(t), \quad U(0) = I_n \\ \bar{H}(t) &= H_0 + H_c(t) \end{aligned} \quad (1)$$

The Hamiltonian consists of two terms: the first,  $\bar{H}(t)$ , is the *nominal*, a known unperturbed term with a (usually) constant drift term,  $H_0$ , and a time-varying control term,  $H_c(t)$ , which depends on  $m$  control variables  $v_1(t), \dots, v_m(t)$ . In many cases  $H_c(t)$  is linear in the control variables, *i.e.*,  $H_c(t) = \sum_{j=1}^m v_j(t)H_j$ . The corresponding nominal (unperturbed) unitary, denoted by  $\bar{U}(t)$ , evolves from,

$$i\dot{\bar{U}}(t) = \bar{H}(t)\bar{U}(t), \quad \bar{U}(0) = I_n \quad (2)$$

The nominal fidelity to achieve a unitary target  $W$  is,

$$F_{\text{nom}} = |\text{tr}(W^\dagger \bar{U}(T)/n)|^2 \in [0, 1] \quad (3)$$

The second term,  $\tilde{H}(t)$ , is an uncertain *perturbation* such that,

$$\left\{ \tilde{H}(t), t \in [0, T] \right\} \in \mathcal{H}_{\text{unc}} \quad (4)$$

where the characteristics of  $\mathcal{H}_{\text{unc}}$  are known, *e.g.*, norm bounds and/or probability distributions on Hamiltonian parameters or parts thereof. To assess the effect of a specified Hamiltonian perturbation on the nominal system, it is natural to compare the final-time perturbed system unitary  $U(T)$  evolving from (1) with the target unitary  $W$ . One such performance measure is the worst-case fidelity,

$$F_{\text{wc}} = \min_{\tilde{H} \in \mathcal{H}_{\text{unc}}} |\text{tr}(W^\dagger U(T)/n)|^2, \quad (5)$$

As described in [23],  $F_{\text{wc}}$  can be approximated by sampling over the uncertainty set, and for small errors a convex approximation along with a complementary optimization can provide more confidence towards having found the worst-case fidelity. Similar results hold for the average-case fidelity. However, as more error types and sources are discovered, or others are considered, sampling or convex approximations can get computationally burdensome, particularly if multiple error sources have to be simultaneously evaluated.

## III. ANALYSIS OF ROBUSTNESS

To analyze the effect of perturbations we view the system evolution via the *interaction* unitary between the nominal and perturbed unitaries [2–16]. Specifically, let  $U(t) = \bar{U}(t)R(t)$

where  $R(t)$  is the interaction unitary which evolves from,

$$\begin{aligned} i\dot{R}(t) &= G(t)R(t), \quad R(0) = I_n \\ G(t) &= \bar{U}(t)^\dagger \tilde{H}(t) \bar{U}(t) \end{aligned} \quad (6)$$

with  $G(t)$  referred to as the *interaction Hamiltonian*. The worst-case fidelity (5) is then equivalently given by,

$$F_{\text{wc}} = \min_{\tilde{H} \in \mathcal{H}_{\text{unc}}} |\text{tr}(W^\dagger \bar{U}(T)R(T)/n)|^2 \quad (7)$$

Deviations from the nominal are now captured by the deviation of  $R(T)$  from identity, *i.e.*, if  $R(T) \approx I_n$  then  $F_{\text{wc}} \approx F_{\text{nom}}$ . This approximation can be made precise by utilizing the standard method of averaging [1] which shows a means for significantly reducing the size of  $\|R(T) - I_n\|$  by controlling the *nominal trajectory*  $\bar{U}(t), t \in [0, T]$ . The following result is established in Appendix §A.

**Theorem 1 (Averaging Analysis)** *For the unitary system (1)-(2), denote by  $G_{\text{avg}}$  the time-averaged Hamiltonian,*

$$G_{\text{avg}} = \frac{1}{T} \int_0^T \bar{U}(t)^\dagger \tilde{H}(t) \bar{U}(t) dt \quad (8)$$

*Assume that amongst the properties of the uncertainty set (4) is the bound,  $\|\tilde{H}(t)\| \leq \delta$  for a specified norm. Under these conditions,*

$$\text{if } \|G_{\text{avg}}\| \leq \bar{\gamma} \delta \quad \text{and} \quad \|G(t) - G_{\text{avg}}\| \leq \tilde{\gamma} \delta,$$

$$\text{then as } F_{\text{nom}} \rightarrow 1, \quad (9)$$

$$F_{\text{wc}} \rightarrow F_{\text{nom}} - (\mathcal{O}\{\bar{\gamma}(\delta T)\} + \mathcal{O}\{\tilde{\gamma}(\delta T)^2\})^2$$

Theorem 1 shows that if the nominal performance is acceptable, *i.e.*,  $F_{\text{nom}} \approx 1$ , and the mean ( $\bar{\gamma}$ ) and deviation ( $\tilde{\gamma}$ ) of the *time-averaged Hamiltonian* (effectively the first term in the Magnus expansion of  $R(T)$ , the interaction unitary) are sufficiently small, then significant robustness about the nominal accrues. And of note,  $\delta T$  need not be small. However, if only the mean  $\bar{\gamma}$  can be made very small, then at most only higher order errors are present. The worst-case fidelity summarized in (9) follows from an explicit bound as part of the derivation provided in Appendix §A.

The analysis result above is readily extended to systems with multiple *additive* error sources and associated time-averaged Hamiltonians, that is,

$$\begin{aligned} \tilde{H}(t) &= \sum_{\ell=1}^L \tilde{H}_\ell(t), \quad \tilde{H}_\ell(t) \in \mathcal{H}_{\text{unc}}^\ell \\ G_{\text{avg}}^\ell &= \frac{1}{T} \int_0^T \bar{U}(t)^\dagger \tilde{H}_\ell(t) \bar{U}(t) dt \end{aligned} \quad (10)$$

Large values of any  $G_{\text{avg}}^\ell$  indicates a source of potentially disruptive errors. Thus each of the time-averaged Hamiltonians can be used to assess the impact on the nominal design of any anticipated or suspected errors *without having to run full sim-*

ulations and without resorting to a possibly computationally burdensome worst-case error evaluation (5).

These properties of the time-averaged Hamiltonian show in general how the *trajectory* of the nominal propagator can establish robustness. As there are many pathways via control that achieve the same fidelity level [17–22], there is expected to be considerable freedom in choosing a pathway that simultaneously achieves a high fidelity nominal response *and* minimizes the size of each of the time-averaged Hamiltonians  $G_{\text{avg}}^\ell$ . The freedom discussed arises from the ability to roam over the null space at the top of the fidelity landscape.

## IV. ROBUST CONTROL SYNTHESIS

### A. Synthesis criteria

Theorem 1 also provides design criteria to *synthesize* a robust control. Specifically, the *nominal* propagator  $\bar{U}(t), t \in [0, T]$  should have the following features:

1. the final time nominal unitary is very close to the target  $W$ , *i.e.*, the nominal fidelity  $F_{\text{nom}} \approx 1$  (3).
2. each time-averaged Hamiltonian perturbation (10) is small:  $G_{\text{avg}}^\ell \approx 0$ .

These two goals, which place simultaneous demands on the *nominal trajectory*,  $\bar{U}(t), t \in [0, T]$ , has been presented in various forms in [8–16].

Here we provide another version formulated as a multicriterion optimization problem. The synthesis (or design) variables are the controls  $v_j(t), j = 1 : m, t \in [0, T]$  which are constrained to a set  $\mathcal{V}_{\text{ctrl}}$  reflecting any limitations imposed by the control actuators, *e.g.*, magnitude, sampling rate, bandwidth limitations from actuator dynamics, linear combination of basis functions, *e.g.*, for a piece-wise-constant constraint the basis functions are pulses, *etc.*

### B. Multicriterion optimization

To satisfy the two synthesis criteria arising from Theorem 1, we form the following generic *multicriterion* optimization problem,

$$\begin{aligned} & \text{minimize } \Phi(v) = \{1 - F_{\text{nom}}(v), J_{\text{rbst}}(v)\} \\ & \text{subject to } J_{\text{rbst}}(v) = \sum_{\text{unc}} \delta_{\text{unc}} \|\mathcal{A}_{\text{unc}}(v) S_{\text{unc}}\|_{\text{unc}} \quad (11) \\ & \quad v \in \mathcal{V}_{\text{ctrl}} \end{aligned}$$

where  $v$  is the vector of control variables,  $J_{\text{rbst}}(v)$  is a robustness measure reflecting the magnitude of the time-averaged Hamiltonians in (18), and the objective notation  $\{\cdot, \cdot\}$  is meant to denote the possible trade-off between the two objectives [24].

In a later section, where we describe some common types of uncertainty, we show that all of these result in a robustness

measure  $J_{\text{rbst}}(v)$  which has the generic form shown. Specifically, the matrix  $\mathcal{A}_{\text{unc}}(v)$  will be seen to capture the interaction between the nominal unitary trajectory and the uncertainty, the matrix  $S_{\text{unc}}$ , the norm  $\|\cdot\|_{\text{unc}}$  and associated error bound  $\delta_{\text{unc}}$  all follow from the probabilistic or deterministic uncertainty character. With a single uncertainty, or several with near equal bounds, it is not always necessary to include the bounding variables, in which case they are effectively absorbed into the robustness measure.

### C. Two-stage algorithm

As alluded to earlier, at the top of the control landscape where  $F_{\text{nom}}(v) = 1$ , the gradient  $\nabla_v F_{\text{nom}}(v) = 0$ , there is potentially a large null space [17–22]. This *roaming* freedom at the top of the landscape derives from the structure of the Hessian of the nominal fidelity,  $\nabla_v^2 F_{\text{nom}}(v)$ , which is negative semidefinite and low-rank, and this can only have a modest number of eigenvectors with negative eigenvalues (*i.e.*, these specify the portion of the control that maximizes the fidelity measure). In turn, the remaining, often very large null space, with associated zero eigenvalues, can serve as a space to project the system disturbances. Ergo, one iterative path to finding a solution to (11) is to first maximize only the nominal fidelity  $F_{\text{nom}}(v)$ . When this fidelity crosses a high threshold,  $f_0 \approx 1$ , then switch to minimizing the robustness measure  $J_{\text{rbst}}(v)$  while keeping the fidelity above  $f_0$ . Specifically, we utilize the following two stage algorithm:

$$\begin{aligned} & \text{Stage 1 maximize only } F_{\text{nom}}(v) \text{ until } F_{\text{nom}}(v) \geq f_0 \\ & \text{Stage 2 minimize } J_{\text{rbst}}(v) \text{ while } F_{\text{nom}}(v) \geq f_0 \end{aligned} \quad (12)$$

The uncertainty-free optimization in Stage 1 can be done by many different gradient ascent methods. For Stage-2, when  $F_{\text{nom}}(v) \geq f_0$ , we show in Appendix §B that finding an optimal control increment  $\tilde{v}$  to solve (12) can be recast *exactly* as a convex optimization problem. This approach differs from earlier works which used the properties of the null space at high fidelity directly [17–22].

In particular, during Stage-2, let fidelity and robustness at the current control  $v$  be denoted by  $F_{\text{nom}}$  and  $J_{\text{rbst}}$ . For a change in controls from  $v$  to  $v + \tilde{v}$ , by approximating both the fidelity and robustness changes by quadratic functions (gradients and Hessians) in the control increments  $\tilde{v}$ , the next control increment can be found by solving the following optimization problem:

$$\begin{aligned} & \text{minimize } \tilde{v}^T \tilde{v} + \alpha (J_{\text{quad}}(\tilde{v}) - J_{\text{rbst}}) \\ & \text{subject to } F_{\text{quad}}(\tilde{v}) \geq f_0 \end{aligned} \quad (13)$$

where

$$\begin{aligned} F_{\text{quad}}(\tilde{v}) &= F_{\text{nom}} + \nabla F_{\text{nom}}^T \tilde{v} + \tilde{v}^T \nabla^2 F_{\text{nom}} \tilde{v} / 2 \\ J_{\text{quad}}(\tilde{v}) &= J_{\text{rbst}} + \nabla J_{\text{rbst}}^T \tilde{v} + \tilde{v}^T \nabla^2 J_{\text{rbst}} \tilde{v} / 2 \end{aligned} \quad (14)$$

The objective is a trade-off between a small control increment  $\tilde{v}$  and a  $J_{\text{rbst}}$  decrease (robustness increase) with robustness weight  $\alpha > 0$ . The constraint keeps the nominal fidelity higher than  $f_0 \approx 1$ . Although (13) is not always a convex optimization, using [24, App.B] as shown in Appendix §B, the increment  $\tilde{v}$  can be found efficiently by solving for the two variables  $\gamma, \lambda \in \mathbb{R}$  in the associated (convex) dual optimization problem,

$$\begin{aligned} & \text{maximize } \gamma \\ & \text{subject to } \lambda \geq 0 \\ & \begin{bmatrix} I - \lambda \nabla^2 F_{\text{nom}} + \alpha \nabla^2 J_{\text{rbst}} & \alpha \nabla J_{\text{rbst}} - \lambda \nabla F_{\text{nom}} \\ (\alpha \nabla J_{\text{rbst}} - \lambda \nabla F_{\text{nom}})^T & -2\lambda(F_{\text{nom}} - f_0) - \gamma \end{bmatrix} \geq 0 \end{aligned} \quad (15)$$

From  $\lambda$  the control increment is given by,

$$\tilde{v} = - (I - \lambda \nabla^2 F_{\text{nom}} + \alpha \nabla^2 J_{\text{rbst}})^{-1} (\alpha \nabla J_{\text{rbst}} - \lambda \nabla F_{\text{nom}}) \quad (16)$$

In addition, if the threshold is maintained, *i.e.*,  $F_{\text{quad}}(\tilde{v}) > f_0$ , then  $J_{\text{rbst}}$  can never increase. Figures 1-2 show two basic examples of the two-stage algorithm that exhibit the topological property at high fidelity.

## V. UNCERTAINTY MODELING

In this section several representative Hamiltonian uncertainty sets (4) are presented along with their corresponding robustness measures  $J_{\text{rbst}}$  (11). The uncertainty is represented by unknown but bounded Hamiltonian parameters that can be constant or time varying, and either deterministic or probabilistic. The models are canonical, their main purpose being to capture uncertainty obtained from the underlying physics supported by data. If they are too conservative in relation to the control resources, then robustness will be compromised.

A few of the uncertainty models described in this section are displayed in Table-I. Clearly there are many combinations and variations of these elementary uncertainty sets that can be formulated. Selected numerical examples are presented in §VI. Additional uncertainty models are presented in Appendix §C including multiplicative control noise, actuator dynamic uncertainty, cross-coupling, open bipartite systems, and Lindblad uncertainty. A few additional numerical examples are in Appendix §D.

### A. Piece-wise-constant (PWC) control

To make the uncertainty modeling procedures precise, we start with the minimal restriction that the ideal control actuator produces  $N$  perfect pulses of width  $T/N$ . This motivates switching to a discrete-time picture, where now  $t = 1 : N$  denotes these  $N$  uniformly spaced intervals. Equivalently, each of the  $m$  controls in (1) are piece-wise-constant (PWC) with magnitudes  $v_{tj}, j = 1 : m, t = 1 : N$ ; these  $mN$  magnitudes are the design variables. (In general the PWC controls could be phases, frequencies or weights in some basis.)

The nominal propagator evolution is then determined by a product of  $N$  unitaries, expressed recursively for  $t = 1 : N$  as,

$$\begin{aligned} \bar{U}_t &= e^{-i(T/N)\bar{H}_t}\bar{U}_{t-1}, \bar{U}_0 = I_n \\ \bar{H}_t &= H_0 + H_c(v_t), \quad v_t = \{v_{tj}, j = 1 : m\} \end{aligned} \quad (17)$$

The discrete-time version of each of the  $L$  time-averaged Hamiltonians in (10) is obtained at an appropriate sampling rate for the uncertainty characteristics. This rate is not necessarily the same as the control PWC rate of  $T/N$ . Let the sampling rate for averaging (and simulation) be  $T/M$  with  $M \geq N$  and for consistency  $M/N$  is an integer. Then,

$$\begin{aligned} \tilde{H}_t &= \sum_{\ell=1}^L \tilde{H}_{\ell t}, \quad \tilde{H}_{\ell t} \in \mathcal{H}_{\text{unc}}^\ell \\ G_{\text{avg}}^\ell &= \frac{1}{M} \sum_{t=1}^M \bar{U}_t^\dagger \tilde{H}_{\ell t} \bar{U}_t \end{aligned} \quad (18)$$

For ease of notation we use  $t$  as the sample time index if it is clear in the context which rate applies, *i.e.*,  $T/N$  for PWC control (17) and  $T/M$  for uncertainty and averaging (18).

### B. Uncertain constant Hamiltonian parameter

A common form of an uncertain perturbation is one composed of the sum of products of unknown but bounded *constant* parameters and known (possibly time-varying) Hamiltonians. The resulting Hamiltonian uncertainty set is,

$$\mathcal{H}_{\text{unc}} = \left\{ \tilde{H}_t = \sum_{\ell=1}^L \theta_\ell B_{\ell t} \left| \begin{array}{l} \vec{\theta} = [\theta_1 \ \dots \ \theta_L]^T \in \Theta \\ \|B_{\ell t}\| \leq 1, t = 1 : M \end{array} \right. \right\} \quad (19)$$

The corresponding time-averaged Hamiltonian is,

$$G_{\text{avg}} = \frac{1}{M} \sum_{t=1}^M \sum_{\ell=1}^L \theta_\ell \bar{U}_t^\dagger B_{\ell t} \bar{U}_t \quad (20)$$

### C. Bounded parameters

To model the effect of uncertain but bounded Hamiltonian parameters, assume that the  $L \times 1$  vector of parameters  $\vec{\theta}$  belongs to one of the following three uncertainty sets:

$$\begin{aligned} \text{peak} & \quad \Theta_\infty = \{\|\vec{\theta}\|_\infty \leq \delta_\infty\} \\ \text{energy} & \quad \Theta_2 = \{\|\vec{\theta}\|_2 \leq \delta_2\} \\ \text{covariance} & \quad \Theta_{\text{prob}} = \left\{ \begin{array}{l} \vec{\theta} \text{ zero-mean} \\ \text{cov } \vec{\theta} = C \geq 0 \end{array} \right\} \end{aligned} \quad (21)$$

One way to see the effect of the uncertain parameters is to stack *all*  $n^2$  elements of  $G_{\text{avg}}$  in (8) into the vector  $\vec{G}_{\text{avg}}$  re-

Uncertainty Type	Uncertainty Set $\tilde{H}_t \in \mathcal{H}_{\text{unc}}$	Robustness Measure $J_{\text{rbst}} = \delta_\mu \ \mathcal{A}S\ _\mu$
Constant parameters (magnitude bounded) (see §VB)	$\tilde{H}_t = \sum_{\ell=1}^L \theta_\ell B_{\ell t}$ $B_{\ell t}$ known $\ \tilde{\theta}\ _\mu \leq \delta_\mu$	$\mathcal{A} = [\vec{A}_1 \ \dots \ \vec{A}_L] \ (n^2 \times L)$ $A_\ell = (1/M) \sum_{t=1}^M \bar{U}_t^\dagger B_{\ell t} \bar{U}_t, \ell = 1 : L$ $\ \tilde{\theta}\ _\infty \leq \delta_\infty \Rightarrow \mu = \infty, S = I_L$ $\ \tilde{\theta}\ _2 \leq \delta_2 \Rightarrow \mu = 2, S = I_L$ $\text{cov } \tilde{\theta} = C \Rightarrow \mu = \text{fro}, S = \sqrt{C}$
Constant Hamiltonian (energy-bounded) (see §VE)	$\tilde{H}$ constant, $\ \tilde{H}\ _{\text{fro}} \leq \delta$ equivalent to: $\tilde{H} = \sum_{i=1}^{n^2} \theta_i \Gamma_i, \ \tilde{\theta}\ _2 \leq \delta$ $[\vec{\Gamma}_1 \ \dots \ \vec{\Gamma}_{n^2}], (n^2 \times n^2)$ unitary	$\mathcal{A} = [\vec{A}_1 \ \dots \ \vec{A}_{n^2}] \ (n^2 \times n^2)$ $A_i = \frac{1}{M} \sum_{t=1}^M \bar{U}_t^\dagger \Gamma_i \bar{U}_t, i = 1 : n^2$ $S = I_{n^2}, \mu = 2$
Time-varying parameter (band limited, stationary) (see §VF)	$\tilde{H}_t = \theta_t B_t$ band-limited constraint: $\tilde{\theta} = \delta (\mathcal{K} \vec{w} / \ \mathcal{K}\ _{\text{fro}}), \text{cov } \vec{w} = I_M$ $\mathcal{K}$ is Toeplitz noise filter matrix	$\mathcal{A} = [\vec{A}_1 \ \dots \ \vec{A}_M] \ (n^2 \times M)$ $A_t = \bar{U}_t^\dagger B_t \bar{U}_t / M, t = 1 : M$ $S = \mathcal{K} / \ \mathcal{K}\ _{\text{fro}}, \mu = \text{fro}$

TABLE I. Table summarizing three common classes of Hamiltonian uncertainties and associated robustness measures (11) as described in §V. **Key:** system dimension is  $n$ , PWC control sample rate is  $T/N$ ; averaging/simulation sample rate is  $T/M$  with  $M/N$  an integer.

sulting in,

$$\vec{G}_{\text{avg}} = \mathcal{A} \tilde{\theta} \begin{cases} \mathcal{A} = [\vec{A}_1 \ \dots \ \vec{A}_L] \in \mathbb{C}^{n^2 \times L} \\ A_\ell = (1/M) \sum_{t=1}^M \bar{U}_t^\dagger B_{\ell t} \bar{U}_t \in \mathbb{C}^{n \times n} \end{cases} \quad (22)$$

Since  $\vec{G}_{\text{avg}}$  is linear in  $\tilde{\theta}$ , the robustness measures corresponding to the sets in (21) follow directly from the induced norm properties, *i.e.*,

$$\begin{aligned} \tilde{\theta} \in \Theta_\infty &\Rightarrow J_{\text{rbst}} = \delta_\infty \|\mathcal{A}\|_\infty = \delta_\infty \max_{i=1:n^2} \sum_{\ell=1}^L |\vec{A}_{\ell i}| \\ \tilde{\theta} \in \Theta_2 &\Rightarrow J_{\text{rbst}} = \delta_2 \|\mathcal{A}\|_2 \\ \tilde{\theta} \in \Theta_{\text{prob}} &\Rightarrow J_{\text{rbst}} = \text{tr}(\text{cov } G_{\text{avg}}) = \|\mathcal{A} \sqrt{C}\|_{\text{fro}}^2 \end{aligned} \quad (23)$$

These robustness measures reflect individual terms in (11), the  $\mathcal{A}$ -matrix being the same for all three cases above. For the two deterministic sets ( $\Theta_\infty, \Theta_2$ ) the effective  $S$ -matrix is simply  $S = I_L$  with  $\mu = \infty$  and  $\mu = 2$ , respectively. For the probabilistic set ( $\Theta_{\text{prob}}$ ),  $S = \sqrt{C}$  with  $\mu = \text{fro}$ . Clearly more nuanced uncertainty configurations are possible, *e.g.*, mixing matrix and vector norms such as  $J_{\text{rbst}} = \max_{\theta \in \Theta_2} \|G_{\text{avg}}\|_\infty$ , and so on. In addition, in a sum of measures, each measure could differ, or for groups of parameters each might have different types of bounds.

#### D. Bias and drift

Although  $\tilde{\theta}$  in the instances described is a bounded uncertain constant, the specific value within the bound can vary over each run time interval  $t \in [0, T]$ . Thus the uncertainty set (19) is describing parameters which can change abruptly from run-

to-run. If, however,  $\tilde{\theta}_t$  is slowly drifting in each run, and is memoryless from run-to-run, then for each of  $L$  parameters a more suitable model for  $t = 1 : M$  is,

$$\theta_{\ell,t} = h_t^T c_\ell, \quad h_t = \frac{1}{M-1} \begin{bmatrix} M-t \\ t-1 \end{bmatrix}, \quad c_\ell = \begin{bmatrix} a_\ell \\ b_\ell \end{bmatrix} \quad (24)$$

In each run  $a_\ell$  is the initial value and  $b_\ell$  is the final value. Assuming that for some norm each  $c_\ell$  is independently bounded by  $\|c_\ell\| \leq \delta_\ell$ , then following (22)-(23), the robustness measure is,

$$J_{\text{rbst}} = \sum_{\ell=1}^L \delta_\ell \|\mathcal{A}_\ell\| \begin{cases} \mathcal{A}_\ell = \sum_{t=1}^M \vec{A}_{\ell,t} h_t^T \in \mathbb{C}^{n^2 \times 2} \\ A_{\ell,t} = \bar{U}_t^\dagger B_{\ell,t} \bar{U}_t \end{cases} \quad (25)$$

#### E. Uncertain constant energy-bounded Hamiltonian

An interesting example of a constant Hamiltonian perturbation is the set of uncertain energy-bounded constant Hamiltonians,

$$\mathcal{H}_{\text{unc}} = \{\tilde{H} \text{ constant}, \|\tilde{H}\|_{\text{fro}} \leq \delta\} \quad (26)$$

Clearly  $\tilde{H}$  is arbitrary other than subject to an ‘‘energy-like’’ bound. Consequently, an equivalent uncertainty set is,

$$\mathcal{H}_{\text{unc}} = \left\{ \tilde{H} = \sum_{i=1}^{n^2} \theta_i \Gamma_i \left| \begin{array}{l} [\vec{\Gamma}_1 \ \dots \ \vec{\Gamma}_{n^2}] \in \mathcal{U}(n^2) \\ \|\tilde{\theta}\|_2 \leq \delta \end{array} \right. \right\} \quad (27)$$



where  $\Gamma_i, i = 1 : n^2$  is any orthonormal basis set for  $n \times n$  Hermitian matrices, and where the vector  $\vec{\theta} \in \mathbb{R}^{n^2}$ , bounded in the two-norm by  $\delta$ , consists of all the constant coefficients  $\theta_i \in \mathbb{R}, i = 1 : n^2$ . The equivalence follows from the fact that  $\|\tilde{H}\|_{\text{fro}} = \|\text{vec}(\tilde{H})\|_2$  along with the induced norm property of the vector two-norm. Thus for any orthonormal (Hermitian) basis, the real coefficients are equivalent to all possible entries in *any constant*  $\tilde{H}$  such that  $\|\tilde{H}\|_{\text{fro}} \leq \delta$ . It follows that for an energy bounded parameter uncertainty the appropriate robustness measure is of the same form of (23), *i.e.*,

$$J_{\text{rbst}} = \delta \|\mathcal{A}\|_2 \begin{cases} \mathcal{A} = [\vec{A}_1 \ \cdots \ \vec{A}_{n^2}] \\ A_i = (1/M) \sum_{t=1}^M \bar{U}_t^\dagger \Gamma_i \bar{U}_t \end{cases} \quad (28)$$

where the  $S$ -matrix is simply  $I_{n^2}$ , the identity matrix.

### F. Uncertain time-varying Hamiltonian parameter

Uncertain parameter time variation can arise in a number of forms depending on the underlying physics. Here we pose a few generic uncertainty models which capture the effects of limited-bandwidth and stationary noise.

#### 1. Limited bandwidth

Let  $\theta_t, t = 1 : M$  denote an uncertain bounded *time-varying* parameter associated with the *single* perturbation  $\tilde{H}_t = \theta_t B_t$  where  $B_t$  is known and typically normalized so that  $\|B_t\| \leq 1$ . To capture limited-bandwidth, assume that  $\theta_t$  is the output of a ‘‘filter’’ driven by a bounded sequence  $w_t, t = 1 : N$ , where the filter is well represented as a linear-time-varying (LTV) system with causal (convolution) dynamics [25],

$$\theta_t = \sum_{\tau=1}^t K_{t\tau} w_\tau \quad (29)$$

Since causality implies that  $K_{t\tau} = 0$  for  $\tau > t$ , the vector of time-varying parameters can be expressed by  $\vec{\theta} = \mathcal{K}\vec{w}$  with  $\mathcal{K}$  the  $M \times M$  *block-lower-triangular* matrix,

$$\mathcal{K} = \begin{bmatrix} K_{11} & & & \\ K_{22} & K_{21} & & \\ \vdots & \ddots & \ddots & \\ K_{MM} & \cdots & K_{M2} & K_{M1} \end{bmatrix} \quad (30)$$

If the filter is linear-time-invariant (LTI) then (29) becomes  $\theta_t = \sum_{\tau=1}^t K_{t-\tau} w_\tau$  from which it follows that the matrix  $\mathcal{K}$

is lower-triangular Toeplitz, *i.e.*,

$$\mathcal{K} = \begin{bmatrix} K_1 & & & \\ K_2 & K_1 & & \\ \vdots & \ddots & \ddots & \\ K_M & \cdots & K_2 & K_1 \end{bmatrix} \quad (31)$$

For an LTI filter the first column above is the impulse response of the filter dynamics.

#### 2. Stationary noise modeling

For either LTV or LTI dynamics, assume further that  $\vec{w}$ , the noise filter input, is a zero-mean stationary sequence with unit covariance  $\text{cov}(\vec{w}) = I_M$ . Under these conditions, the Hamiltonian uncertainty set is,

$$\mathcal{H}_{\text{unc}} = \left\{ \tilde{H}_t = \theta_t B_t \left| \begin{array}{l} \vec{\theta} = \mathcal{K}\vec{w}, \vec{w} \text{ zero-mean} \\ \text{cov}(\vec{w}) = I_M \end{array} \right. \right\} \quad (32)$$

The corresponding  $n^2 \times 1$  vector of the time-averaged Hamiltonian is,

$$\vec{G}_{\text{avg}} = \mathcal{A}\mathcal{K}\vec{w} \begin{cases} \mathcal{A} = [\vec{A}_1 \ \cdots \ \vec{A}_N] \ (n^2 \times M) \\ A_t = \bar{U}_t^\dagger B_t \bar{U}_t / M \end{cases} \quad (33)$$

Consequently, for a single error source the output magnitude level is subsumed in the noise filter  $\mathcal{K}$ . (Explicit bound shown in Table-I.) For multiple time-varying perturbations of the form  $\tilde{H}_{\ell t} = \theta_{\ell t} B_{\ell t}, \ell = 1 : L$  with independent time-varying parameters  $\vec{\theta}_\ell = \mathcal{K}_\ell \vec{w}_\ell$ , the robustness measure is the sum,

$$J_{\text{rbst}} = \sum_{\ell=1}^L \|\mathcal{A}_\ell S_\ell\|_{\text{fro}}^2 \begin{cases} \mathcal{A}_\ell = [\vec{A}_{\ell 1} \ \cdots \ \vec{A}_{\ell M}] \\ A_{\ell t} = \bar{U}_t^\dagger B_{\ell t} \bar{U}_t \\ S_\ell = \mathcal{K}_\ell \end{cases} \quad (34)$$

with  $(S_\ell, \mathcal{A}_\ell)$  correspondingly defined as previously per the characteristics of each perturbation and where output power of each time-varying parameter is contained in each  $\mathcal{K}_\ell$ . As shown in Appendix §C3, in this instance the robustness measure can be formed in the frequency domain using a filter function as in [8–16].

## VI. NUMERICAL EXAMPLES

The purpose of these numerical examples is to illustrate the averaging theory in conjunction with the two-stage optimization as outlined in (12)–(16) and further described in Appendix §B. The examples all demonstrate ready access to the null space at the top of the control landscape which is essential for robust control. The focus throughout is (mostly) on a few basic single qubit systems. Appendices §C and §D contain additional uncertainty models and numerical examples.

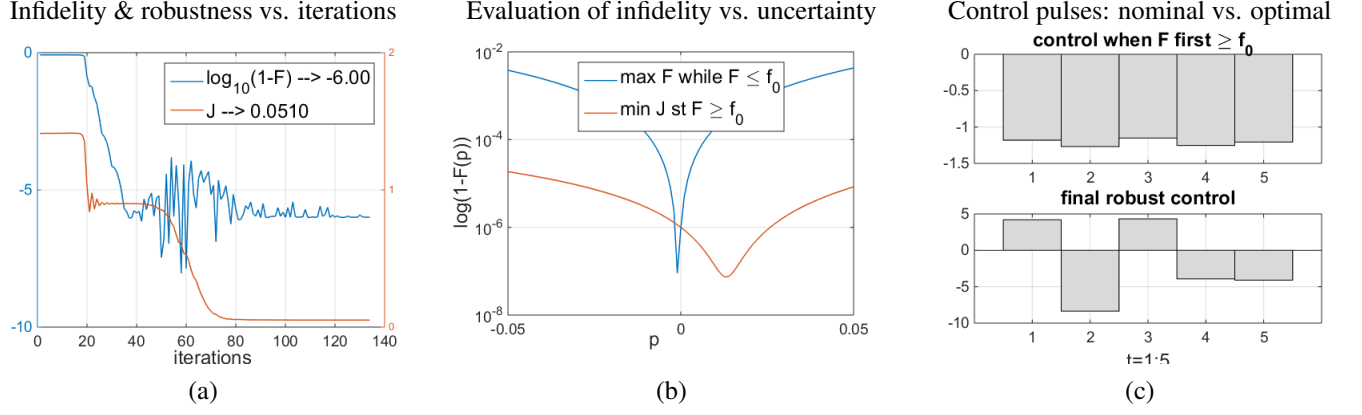


FIG. 1. Uncertain constant parameter  $H_t = v_t \sigma_x + (1 + \theta) \sigma_z$ .

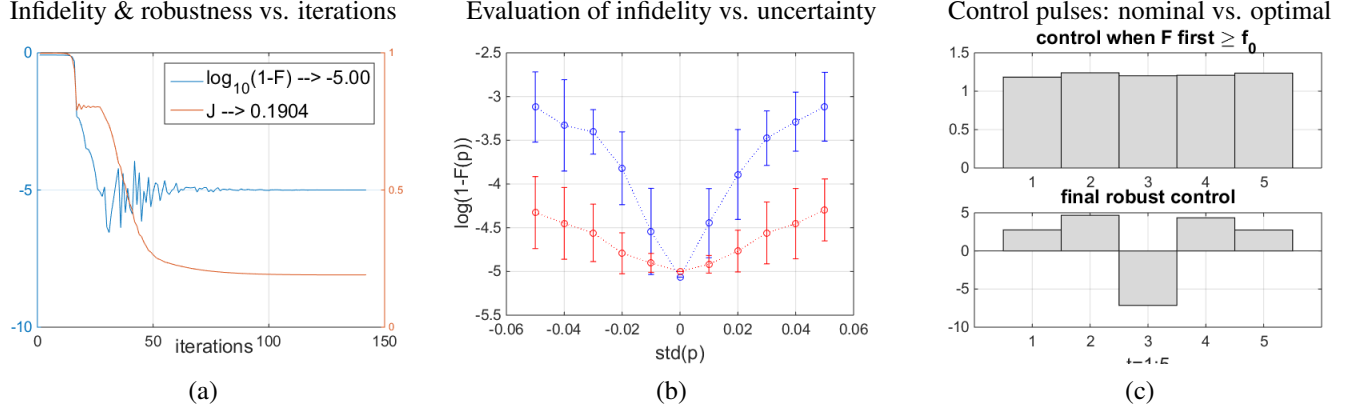


FIG. 2. Uncertain time-varying parameter  $H_t = v_t \sigma_x + (1 + \theta_t) \sigma_z$ .

### A. Constant uncertain parameter

Denote by  $\theta$  an uncertain real parameter in the drift term of the single qubit Hamiltonian system,

$$H_t = v_t \sigma_x + (1 + \theta) \sigma_z \quad \begin{cases} \bar{H}_t = v_t \sigma_x + \sigma_z \\ \tilde{H}_t = \theta \sigma_z, -\delta \leq \theta \leq \delta \end{cases} \quad (35)$$

where  $v_t, t = 1 : N$  are the  $N$  piece-wise-constant (PWC) control pulse magnitudes of the (single) control variable over the normalized time interval  $[0, 1]$  with uniform pulse widths  $1/N$ . Noting that the parameter uncertainty belongs to the class  $\vec{\theta} \in \Theta_\infty$  from (23), the form of the objective function follows from (11) as,

$$\Phi = \{1 - F_{\text{nom}}, \|\mathcal{A}\|_\infty\} \quad \begin{cases} F_{\text{nom}} = |\text{tr}(W^\dagger \bar{U}_N / 2)|^2 \\ \mathcal{A} = [\vec{A}_1 \cdots \vec{A}_M] \\ A_t = \bar{U}_t^\dagger \sigma_z \bar{U}_t / M \end{cases} \quad (36)$$

Since there is a single parameter, the bound  $\delta$  is not needed in the robustness measure, only for evaluation.

Figure 1(a)-(b)-(c) shows the numerical results using the optimization procedure in (B1)-(B2). The goal is to make a-

bust identity gate ( $W = I_2$ ) with  $N = 5$  PWC control pulses and with averaging over  $M = 50$  uniform samples. For evaluation the uncertain constant parameter range is bounded by  $\delta = 0.05$ . In the first stage of the algorithm (B1), the fidelity threshold is set at  $f_0 = 1 - 10^{-6}$ . During the second stage (B2) the weighting parameter which trades control increment size against robustness decrease ((B6) is set at  $\alpha = 5$ .

Figure 1(a) shows the expected behavior: in the first stage only fidelity error (blue) is minimized. At 37 iterations the threshold  $f_0 = 1 - 10^{-6}$  is reached and robustness minimization (red) begins. In the second stage while the fidelity error fluctuates (blue) around  $1 - f_0$  (these only look large on the log scale) the robustness measure decreases eventually converging to a small value. Figure 1(b) compares the fidelity error vs. uncertain parameter level with the stage-1 optimal control (blue plot at 37 iterations) against the robust control (red at final iteration); the latter exhibiting almost two-orders of magnitude improvement at the extremes of the parameter variation: about 0.99999 in fidelity at  $\theta = \pm 0.05$ .

Figure 1(a) – and in other examples to follow – the topological property of the quantum control landscape at or near the top of the landscape is revealed. Specifically, at high values of fidelity, though the fidelity gradient is very small, the Hessian easily allows “roaming at the top of the landscape.” The re-

sult is that the nominal fidelity stays high while the robustness measure is decreased. This is equivalent to manipulating the unitary trajectory so that fidelity remains high, at or near the top of the landscape, so that the additional control freedom in the available null space can provide robustness [17–22].

A visual inspection of the two pulse sequences in Figure 1(c) offers little insight into why the second sequence produces a significant level of robustness. Though the magnitudes of the robust sequence is much larger, it is not understood at this time what is the *precise* mechanism which achieves such a significant robustness advantage. The basis for understanding provided by Theorem 1 is somewhat coarse: make the time-averaged Hamiltonian small, which clearly occurs.

### B. Additive Hamiltonian parameter noise

For this example we replace the *constant* uncertain parameter  $\theta$  in (35) by  $\theta_t, t = 1 : M$ , a real *time-varying* parameter resulting in the Hamiltonian,

$$H_t = v_t \sigma_x + (1 + \theta_t) \sigma_z \quad (37)$$

We again set  $N = 5$  PWC control pulses,  $M = 50$  noise samples, and the identity target. Here we take the noise to be uniformly random in  $\pm 0.05$  with *two* magnitude changes over the time interval. This noise has a “sinc” spectrum (C4). The resulting robustness measure is given by (C6).

Figure 2(a)-(c) displays the simulation results. The fidelity error and robustness measure plots in Figure 2(a) follow the previous pattern of Figure 1(a); here the switching from fidelity error minimization to robustness minimization occurs at iteration 27 when fidelity exceeds  $f_0 = 1 - 10^{-5}$ . Figure 2(b) compares the fidelity range with the control at switching with the final robust control; the plots show the mean and deviations for 100 random samples at each selected uncertainty magnitude in the range out to  $\pm 0.05$ . Figure 2(c) shows the control pulses at switching and final. Clearly a considerable level of robustness is achieved, over an order of magnitude. Interestingly the robust pulse sequence exhibits a symmetric pattern which suggests some possibly generic means to overcome this type of time-varying uncertainty.

## VII. CONCLUDING REMARKS & OUTLOOK

The approach to robust quantum control presented here rests on two theoretical foundations: the classic method of averaging [1] and the known topological properties of the quantum control landscape [17–22]. Application of the method of averaging directly results in a multicriterion optimization problem consisting of the uncertainty-free fidelity competing with a generic robustness measure, the latter being a time-domain product of a function (or functional) of the controls and the character of the uncertainty (11). Such a product form is ubiquitous in the many applications of the *Small Gain Theorem* [26, 27] and generalizations for various uncertainty

models, *e.g.*, [28, 29]. These require a product in a feedback loop to be small: an uncertainty bound and an uncertainty-free (closed-loop) map. From the averaging theory there naturally arises a quantitative norm measure of a time-averaged Hamiltonian (8) reflective of the interaction between the uncertain perturbation and the uncertainty-free unitary evolution. This is the first term in a Magnus expansion of the interaction representation between the nominal unitary and the uncertainty. If this term is sufficiently small, then at most, only second order error effects can accrue (9). In the case of quantum information sciences for established realizations, the tacit assumption is that the (possibly known or unknown) perturbations are small.

The second theoretical foundation, properties of the control landscape topology, motivated a *two-stage algorithm* (12) for finding the robust control: first, maximize fidelity without regard to uncertainty, then, at a high fidelity threshold, switch to maximizing robustness while maintaining the high uncertainty-free fidelity level. We view the time-domain robustness measures developed here together with the two-stage algorithm to solve the multicriterion problem to be complementary to the frequency-domain filter function measures and approaches in [8–16].

In Appendix §B we showed that by using a quadratic approximation of *both* fidelity and robustness in this region of the control landscape, the task of finding a control increment at each iteration is a convex optimization problem. The actual system fidelity robustness of course is subject to the accuracy of the quadratic approximations.

We derived the specific form of the matrix products in the robustness measure corresponding to many common uncertainties. The examples presented, using our two-stage algorithm, clearly illustrate the known flexibility inherent in the landscape topology at high fidelity. However, a visual inspection of many of the robust control pulse sequences does not offer direct insight into why a significant level of robustness is achieved, *i.e.*, the mechanism involved. In a few cases there are discernible symmetric pulse patterns. Unfortunately the basis for understanding provided by Theorem 1 is somewhat coarse: make the time-averaged Hamiltonian small, *e.g.*, via (11), and yet was shown to operate well. However, there is no guarantee that any particular degree of robustness can be achieved, and the best control action at the top of the landscape would most likely call for a global search, unlike the local procedure utilized in this paper.

It is important to emphasize that the *actual* effectiveness of the resulting optimization as predicted by the averaging theory, or by any other approach, can only be determined by evaluation on the total system with uncertainties included. For either deterministic or probabilistic uncertainty sets, this requires simulating the full system with a sufficient number of samples from the uncertainty sets. Ultimately an experiment is the final proof.

Looking ahead, we see a significant unanswered question: *How is robustness precisely achieved for a quantum system?* What is the underlying mechanism? We mentioned the close connection between the generic form of the robustness measure (11) and the Small Gain Theorem [26, 27]. For robust



linear control the latter (and subsequent variations [28, 29]) have proven to be extraordinarily effective (and capable of revealing the robustness mechanism) even against a large class of uncertainties. Moreover, because the mechanism is understood, and in many cases, comprehensible, it is possible to describe a very large class of uncertainty models which encompass what is anticipated without having to delineate each specific possibility [30]. Why not for quantum? For example, is it possible to build a “standard” set of uncertainty models, each of which captures a large variety of possibilities, thereby leading to a universal set of robust quantum controls? A qualitative generic answer can be understood in terms of the landscape “roaming” feature, *i.e.*, seeking a control where the disturbance has minimal eigenvector projection along the Hessian eigenvectors of negative value. Is this what allows a quantitative understanding of the favorable solutions of the dual problem (15), (B8) such that maximum robustness is achieved at high fidelity? Notwithstanding the latter research direction, the fundamental quantum robustness challenge stated above remains.

#### ACKNOWLEDGMENTS

RLK, GB, and HR acknowledge support from the U.S. Department of Energy (DOE) under STTR Contract No. DE-SC0020618. Additionally, HR acknowledges support from the ARO under Contract No. W911NF-19-0382. The authors thank Daniel Lidar, Jason Dominy, and Robert Bitmead for helpful discussions.

#### REFERENCES

- [1] Jack K. Hale. *Ordinary Differential Equations*. Krieger, second edition, 1980.
- [2] Lorenza Viola and Seth Lloyd. Dynamical suppression of decoherence in two-state quantum systems. *Phys. Rev. A*, 58:2733–2744, Oct 1998.
- [3] Lorenza Viola, Emanuel Knill, and Seth Lloyd. Dynamical decoupling of open quantum systems. *Physical Review Letters*, 82:2417, 1999.
- [4] Gotz S. Uhrig. Keeping a quantum bit alive by optimized  $\pi$ -pulse sequences. *PRL*, 98:100504, 2007.
- [5] Kaveh Khodjasteh and Daniel .A. Lidar. Performance of deterministic dynamical decoupling schemes: Concatenated and periodic pulse sequences. *Phys. Rev. A*, 75:062310, 2007.
- [6] Hui Khoon Ng, Daniel A. Lidar, and John Preskill. Combining dynamical decoupling with fault-tolerant quantum computation. *Phys. Rev. A*, 84:012305, Jul 2011.
- [7] Yuhou Xia, Götz S. Uhrig, and Daniel A. Lidar. Rigorous performance bounds for quadratic and nested dynamical decoupling. *Phys. Rev. A*, 84:062332, Dec 2011.
- [8] Todd J Green, Jarrah Sastrawan, Hermann Uys, and Michael J Biercuk. Arbitrary quantum control of qubits in the presence of universal noise. *New Journal of Physics*, 15(9):095004, sep 2013.
- [9] A. Soare, H. Ball, D. Hayes, J. Sastrawan, M. C. Jarratt, J. J. McLoughlin, X. Zhen, T. J. Green, and M. J. Biercuk. Experimental noise filtering by quantum control. *Nature Physics*, 10(11):825–829, Nov 2014.
- [10] Chingiz Kabytayev, Todd J. Green, Kaveh Khodjasteh, Michael J. Biercuk, Lorenza Viola, and Kenneth R. Brown. Robustness of composite pulses to time-dependent control noise. *Phys. Rev. A*, 90:012316, Jul 2014.
- [11] Gerardo A. Paz-Silva and Lorenza Viola. General transfer-function approach to noise filtering in open-loop quantum control. *Phys. Rev. Lett.*, 113:250501, Dec 2014.
- [12] Harrison Ball, Michael J Biercuk, and Andre R R Carvalho *et al.* Software tools for quantum control: improving quantum computer performance through noise and error suppression. *Quantum Science and Technology*, 6(4):044011, sep 2021.
- [13] Holger Haas, Daniel Puzzuoli, Feihao Zhang, and David G Cory. Engineering effective hamiltonians. *New Journal of Physics*, 21(10):103011, oct 2019.
- [14] Teerawat Chalermputitarak, Behnam Tonekaboni, Yuanlong Wang, Leigh M. Norris, Lorenza Viola, and Gerardo A. Paz-Silva. Frame-based filter-function formalism for quantum characterization and control. *PRX Quantum*, 2:030315, Jul 2021.
- [15] Pascal Cerfontaine, Tobias Hangleiter, and Hendrik Bluhm. Filter functions for quantum processes under correlated noise. *Phys. Rev. Lett.*, 127:170403, Oct 2021.
- [16] Xiaodong Yang, Xinfang Nie, Tao Xin, Dawei Lu, and Jun Li. Quantum control for time-dependent noise by inverse geometric optimization. *ArXiv e-prints*, 2022.
- [17] H. Rabitz, M. Hsieh, and C. Rosenthal. Quantum optimally controlled transition landscapes. *Science*, 303, 2004.
- [18] Tak-San Ho, Jason Dominy, and Herschel Rabitz. Landscape of unitary transformations in controlled quantum dynamics. *Phys. Rev. A*, 79(1):013422, Jan 2009.
- [19] Vincent Beltrani, Jason Dominy, Tak-San Ho, and Herschel Rabitz. Exploring the top and bottom of the quantum control landscape. *jcp*, 134(19):194106–194106, May 2011.
- [20] Katharine W. Moore and Herschel Rabitz. Exploring constrained quantum control landscapes. *The Journal of Chemical Physics*, 137(13):134113, 2012.
- [21] David Hocker, Constantin Brif, Matthew D. Grace, Ashley Donovan, Tak-San Ho, Katharine Moore Tibbetts, Rebing Wu, and Herschel Rabitz. Characterization of control noise effects in optimal quantum unitary dynamics. *Physical Review A*, 90(6), Dec 2014.
- [22] Robert L Kosut, Christian Arenz, and Herschel Rabitz. Quantum control landscape of bipartite systems. *Journal of Physics A: Mathematical and Theoretical*, 2019.
- [23] Robert L. Kosut, Matthew D. Grace, and Constantin Brif. Robust control of quantum gates via sequential convex programming. *Phys. Rev. A*, 88:052326, Nov 2013.
- [24] S. Boyd and L. Vandenberghe. *Convex Optimization*. Cambridge University Press, Cambridge, UK, 2004.
- [25] L. Ljung. *System Identification: Theory for the User*. Prentice-Hall, first edition, 1987.
- [26] George Zames. On the input-output stability of time-varying nonlinear feedback systems—part ii: Conditions involving circles in the frequency plane and sector nonlinearities. *IEEE Transactions on Automatic Control*, 11:465–476, 1966.
- [27] C. A. Desoer and M. Vidyasagar. *Feedback Systems: Input-Output Properties*. Academic Press, 1975.
- [28] S. Boyd, L. El Ghaoui, E. Feron, and V. Balakrishnan. *Linear Matrix Inequalities in System and Control Theory*. SIAM studies in applied mathematics: 15, 1994.
- [29] K. Zhou, J. C. Doyle, and K. Glover. *Robust and Optimal Control*. Prentice-Hall, 1996.

- [30] R.L. Kosut, G.C. Goodwin, and M. Polis. Special issue on identification for robust control design. *IEEE Trans. Aut. Contr.*, 37(7), July 1992.
- [31] Ulf Grenander and Gabor Szego. *Toeplitz Forms and Their Applications*. Chelsea Pub. Co., first edition, 1958. Second Edition 1984.

### Appendix A: Proof of Theorem 1

With no loss in generality, set the bounded Hamiltonian perturbation in (4) to  $\dot{H}(t) = \delta B(t)$  where for a specified matrix norm,  $\|B(t)\| = 1$ . The interaction unitary  $R(t), t \in [0, T]$  from (6) then evolves from,

$$\begin{aligned} i\dot{R}(t) &= \delta A(t)R(t), R(0) = I_n \\ A(t) &= \bar{U}(t)^\dagger B(t)\bar{U}(t) \end{aligned} \quad (\text{A1})$$

where  $\bar{U}(t)$  is the nominal (error-free) unitary (2). Define the average interaction unitary,

$$\bar{R}(T) = e^{-i\delta T\langle A \rangle}, \quad \langle A \rangle = \frac{1}{T} \int_0^T A(t) dt \quad (\text{A2})$$

To prove Theorem 1 first requires showing that the interaction unitaries satisfy the following inequalities:

$$\begin{aligned} \|\bar{R}(T) - I\| &\leq e^{\tilde{\gamma}(\delta T)} - 1 \\ \|R(T) - \bar{R}(T)\| &\leq e^{\tilde{\gamma}(\delta T)^2} - 1 \end{aligned} \quad (\text{A3})$$

with  $(\tilde{\gamma}, \tilde{\gamma})$  as defined in (9) of Theorem 1, that is,

$$\tilde{\gamma} = \|\langle A \rangle\|, \quad \tilde{\gamma} = \max_t \|A(t) - \langle A \rangle\| \quad (\text{A4})$$

Using the form of the standard state transformation for averaging analysis described in [1, §V.3] (periodicity, usually assumed, is not needed here) set,

$$\begin{aligned} R(t) &= (I + \delta K(t))V(t) \\ K(t) &= -i \int_0^t (A(\tau) - \langle A \rangle) d\tau \end{aligned} \quad (\text{A5})$$

The matrix  $V(t)$ , which is is not necessarily a unitary, is the solution of,

$$\begin{aligned} i\dot{V} &= \delta (\langle A \rangle + D(t))V, V(0) = I_n \\ D(t) &= \delta (I + \delta K(t))^{-1} (A(t)K(t) - K(t)\langle A \rangle) \end{aligned} \quad (\text{A6})$$

With  $\|A(t)\| \leq 1$ ,  $\|\langle A \rangle\| \leq 1$ , and  $\|A(t) - \langle A \rangle\| \leq \tilde{\gamma}$ , it follows that  $\|K(t)\| \leq \tilde{\gamma}t$ . Additionally,  $K(t) + K(t)^\dagger = 0$  ensures that  $\|(I + \delta K(t))^{-1}\| \leq 1$ . As a result,

$$\begin{aligned} \|D(t)\| &\leq \delta \|A(t)K(t) - K(t)\langle A \rangle\| \\ &\leq 2\delta \|K(t)\| \leq 2\delta\tilde{\gamma}t \end{aligned} \quad (\text{A7})$$

Applying *variation of constants* to (A6) gives,

$$V(t) = \bar{R}(t) - i\delta\bar{R}(t) \int_0^t \bar{R}(\tau)^\dagger D(\tau) V(\tau) d\tau \quad (\text{A8})$$

Introducing the error,

$$E(t) = V(t) - \bar{R}(t) \quad (\text{A9})$$

Substituting into (A8) gives,

$$E(t) = -i\delta\bar{R}(t) \int_0^t \bar{R}(\tau)^\dagger D(\tau) (\bar{R}(\tau) + E(\tau)) d\tau \quad (\text{A10})$$

Since  $\bar{R}(t)$  is a unitary,  $\|\bar{R}(t)\| = 1$ . This together with the previous bound on  $D(t)$  gives,

$$\begin{aligned} \|E(t)\| &\leq 2\tilde{\gamma}\delta^2 \left( \int_0^t \tau d\tau + \int_0^t \tau \|E(\tau)\| d\tau \right) \\ &= \tilde{\gamma}(\delta t)^2 + 2\tilde{\gamma}\delta^2 \int_0^t \tau \|E(\tau)\| d\tau \end{aligned} \quad (\text{A11})$$

Applying the Bellman-Gronwall Lemma together with the fact that  $K(T) = 0$  implies  $R(T) = V(T)$ , and hence,  $E(T) = R(T) - \bar{R}(T)$ , yields the second inequality in (A3). The first inequality in (A3) is a known result which can also be obtained by following the same argument which resulted in the first inequality, now substituting the identity for  $R(t)$  and then applying Bellman-Gronwell.

To prove the main result (9), we need the following relationship established in [22] between fidelity and the Frobenius norm:

$$\begin{aligned} \mathcal{E} &= \min_{|\phi|=1} \|U(T) - \phi W\|_{\text{fro}}^2 = 2n \left( 1 - \sqrt{F} \right) \\ F &= |\text{tr}(W^\dagger U(T)/n)|^2 \\ \phi &= \text{tr}(W^\dagger U(T)/n) / |\text{tr}(W^\dagger U(T)/n)| \end{aligned} \quad (\text{A12})$$

Likewise for the nominal fidelity,

$$\begin{aligned} \mathcal{E}_{\text{nom}} &= \min_{|\phi|=1} \|\bar{U}(T) - \phi W\|_{\text{fro}}^2 = 2n \left( 1 - \sqrt{F_{\text{nom}}} \right) \\ F_{\text{nom}} &= |\text{tr}(W^\dagger \bar{U}(T)/n)|^2 \\ \bar{\phi} &= \text{tr}(W^\dagger \bar{U}(T)/n) / |\text{tr}(W^\dagger \bar{U}(T)/n)| \end{aligned} \quad (\text{A13})$$

To simplify notation we drop the final time  $T$  in all the variables, e.g., let  $U = U(T), \bar{U} = \bar{U}(T)$ , etc.. Applying (A12)-(A13) yields,

$$\begin{aligned} \mathcal{E} &\leq \|U - \bar{\phi}W\|_{\text{fro}}^2 \\ &= \|\bar{U} - \bar{\phi}W + \bar{U}(R - I)\|_{\text{fro}}^2 \quad (\text{using } U = \bar{U}R) \\ &\leq \left( \sqrt{\mathcal{E}_{\text{nom}}} + \|R - I\|_{\text{fro}} \right)^2 \quad (\text{from (A13)}) \end{aligned} \quad (\text{A14})$$

From the definitions of  $\mathcal{E}$  and  $\mathcal{E}_{\text{nom}}$ , the last inequality above is equivalent to,

$$\begin{aligned} F &\geq F_{\text{nom}} - (\tilde{\mathcal{E}}/n)\sqrt{F_{\text{nom}}} + \left( \tilde{\mathcal{E}}/2n \right)^2 \\ \tilde{\mathcal{E}} &= 2\sqrt{\mathcal{E}_{\text{nom}}}\|R - I\|_{\text{fro}} + \|R - I\|_{\text{fro}}^2 \end{aligned} \quad (\text{A15})$$

If  $F_{\text{nom}} \approx 1$ , then  $\mathcal{E}_{\text{nom}} \approx 0$ ,  $\tilde{\mathcal{E}} \approx \|R - I\|_{\text{fro}}^2$  and,

$$F \geq 1 - \|R - I\|_{\text{fro}}^2/n + (\|R - I\|_{\text{fro}}^2/2n)^2 \quad (\text{A16})$$

Thus,

$$\begin{aligned} F &= 1 - \mathcal{O}\{\|R - I\|^2\} \\ &= 1 - \mathcal{O}\{\|\bar{R} - I + R - \bar{R}\|^2\} \\ &= 1 - (\mathcal{O}\{\|\bar{R} - I\|\} + \mathcal{O}\{\|R - \bar{R}\|\})^2 \\ &= 1 - (\mathcal{O}\{\tilde{\gamma}(\delta T)\} + \mathcal{O}\{\tilde{\gamma}(\delta T)^2\})^2 \quad (\text{from (A3)}) \end{aligned} \quad (\text{A17})$$

The last line establishes Theorem 1.

### Appendix B: Two-stage algorithm

With  $m$  PWC controls over  $N$  uniform intervals, the two-stage algorithm in § IVC to find the control variable magnitudes  $v \in \mathbb{R}^{mN}$  can be summarized as follows:

1. **initialize**  $v \in \mathcal{V}_{\text{ctrl}}$ , set a fidelity threshold  $f_0 \approx 1$  and a control increment bound  $\beta$ .

2. **repeat** for  $i = 1, 2, \dots$  until satisfied

(a) **while**  $F_{\text{nom}}(v^i) < f_0$ , **do**

$$v^{i+1} = \arg \min_v \left\{ 1 - F_{\text{nom}}(v) \mid \begin{array}{l} v = v^i + \tilde{v} \in \mathcal{V}_{\text{ctrl}} \\ \|\tilde{v}\| \leq \beta \end{array} \right\} \quad (\text{B1})$$

(b) **while**  $F_{\text{nom}}(v^i) \geq f_0$ , **do**

$$v^{i+1} = \arg \min_v \left\{ J_{\text{rbst}}(v) \mid \begin{array}{l} v = v^i + \tilde{v} \in \mathcal{V}_{\text{ctrl}} \\ \|\tilde{v}\| \leq \beta \\ F_{\text{nom}}(v) \geq f_0 \end{array} \right\} \quad (\text{B2})$$

(c) **stop** when  $J_{\text{rbst}}(v^{i+1}) \approx J_{\text{rbst}}(v^i)$

Since the objective switches from minimizing the uncertainty-free fidelity error,  $1 - F_{\text{nom}}(v)$  to minimizing the robustness measure  $J_{\text{rbst}}(v)$  at the fidelity threshold  $f_0 \approx 1$ , it is expected that the accompanying fidelity gradient  $\nabla F_{\text{nom}}(v)$  will be small. Consequently, the fidelity is best approximated as a quadratic function of the control increment  $\tilde{v}$  in the neighborhood of the current control  $v$ . That is, for a sufficiently small  $\beta$  with  $\|\tilde{v}\| \leq \beta$  the nominal fidelity is approximated as,

$$\begin{aligned} F_{\text{nom}}(v + \tilde{v}) &\approx F_{\text{quad}}(\tilde{v}) \\ &= F_{\text{nom}} + \nabla F_{\text{nom}}^T \tilde{v} + \tilde{v}^T \nabla^2 F_{\text{nom}} \tilde{v}/2 \end{aligned} \quad (\text{B3})$$

where  $F_{\text{nom}}, \nabla F_{\text{nom}}, \nabla^2 F_{\text{nom}}$  are evaluated at  $v$ , the current control. The Hessian  $\nabla^2 F_{\text{nom}}$  may not be negative definite (or negative semidefinite) as would be the case at a global fidelity maximum  $v^*$  where  $F_{\text{nom}}(v^*) = 1$  and  $\nabla F_{\text{nom}}(v^*) = 0$ . However, it is known from topological arguments that at the top, at any global optimum  $v^*$ , the Hessian  $\nabla F_{\text{nom}}(v^*)$  has

$(mN)^* < mN$  negative eigenvalues, the rest are zero, and hence, it is negative semidefinite.

With  $F_{\text{nom}} \approx 1$ , it is to be expected that some number of eigenvalues of  $\nabla^2 F_{\text{nom}}$  are near zero. This motivates replacing  $\nabla^2 F_{\text{nom}}$  with an approximation obtained by setting the small eigenvalues to *exactly* zero. Any control in the null-space defined by the corresponding  $mN - (mN)^*$  eigenvectors can be used for purposes other than keeping  $F_{\text{nom}}(v) \geq f_0$ ; in particular, minimizing the robustness measure. However, the solution method we propose here does not require the Hessian to be positive semidefinite, so there is no need to make a further approximation of the fidelity Hessian.

In the neighborhood of the current control  $v$ , we also approximate the robustness measure as a quadratic in the control increment  $\tilde{v}$ , as follows:

$$\begin{aligned} J_{\text{rbst}}(v + \tilde{v}) &\approx J_{\text{quad}}(\tilde{v}) \\ &= J_{\text{rbst}} + \nabla J_{\text{rbst}}^T \tilde{v} + \tilde{v}^T \nabla^2 J_{\text{rbst}} \tilde{v}/2 \end{aligned} \quad (\text{B4})$$

where  $J_{\text{rbst}}, \nabla J_{\text{rbst}}, \nabla^2 J_{\text{rbst}}$  are evaluated at  $v$ , the current control. Even though the fidelity gradient  $\nabla F_{\text{nom}}$  is small when  $F_{\text{nom}} \approx 1$ , there is no reason to expect that the robustness gradient,  $\nabla J_{\text{rbst}}$ , is small, nor that its Hessian,  $\nabla^2 J_{\text{rbst}}$ , is positive semidefinite. Again, we make no further assumptions or approximations.

In Stage 2, having approximated both fidelity and robustness objectives as a quadratic in control increment  $\tilde{v} \in \mathbb{R}^{mN}$  via (B3)-(B4), we seek the largest decrease in robustness, that is, the largest  $\Delta > 0$  such that there exists  $\tilde{v} \in \mathbb{R}^{mN}$  simultaneously satisfying the three constraints:

$$\tilde{v}^T \tilde{v} \leq \beta, \quad F_{\text{quad}}(\tilde{v}) \geq f_0, \quad J_{\text{quad}}(\tilde{v}) \leq J_{\text{rbst}} - \Delta \quad (\text{B5})$$

Not all these parameters are known: in general would like  $\beta$  to be small to satisfy the quadratic approximations and  $\Delta$  as large as possible. The threshold fidelity can be set to an  $f_0$  near 1, how ‘‘near’’ to 1 may vary per problem. The trade-off amongst the three goals can be expressed by the constrained optimization,

$$\begin{aligned} &\text{minimize} \quad \tilde{v}^T \tilde{v}/2 + \alpha(J_{\text{quad}}(\tilde{v}) - J_{\text{rbst}}) \\ &\text{subject to} \quad F_{\text{quad}}(\tilde{v}) \geq f_0 \end{aligned} \quad (\text{B6})$$

The objective simultaneously reflects the first two goals where  $\alpha > 0$  weighs the robustness decrease ( $-\Delta$ ) relative to the control increment size. Thus the values for  $\beta$  and  $\Delta$  are implicit in the objective; only  $f_0$  and  $\alpha$  are explicitly set. Using the quadratic approximations, the optimization (B6) becomes,

$$\begin{aligned} &\text{minimize} \quad \tilde{v}^T (I + \alpha \nabla^2 J_{\text{rbst}}) \tilde{v} + 2\alpha \nabla J_{\text{rbst}}^T \tilde{v} \\ &\text{subject to} \quad \tilde{v}^T \nabla^2 F_{\text{nom}} \tilde{v} + 2\nabla F_{\text{nom}}^T \tilde{v} + 2(F_{\text{nom}} - f_0) \geq 0 \end{aligned} \quad (\text{B7})$$

At the current control  $v$ , (B7) is not guaranteed to be a convex optimization problem in the increment  $\tilde{v}$ . However, as shown in [24], the dual problem in the two variables  $\lambda, \gamma \in \mathbb{R}$  can be obtained from the linear-matrix-inequality (LMI) constrained

convex optimization,

$$\begin{aligned} & \text{maximize } \gamma \\ & \text{subject to } \lambda \geq 0 \\ & \begin{bmatrix} I - \lambda \nabla^2 F_{\text{nom}} + \alpha \nabla^2 J_{\text{rbst}} & \alpha \nabla J_{\text{rbst}} - \lambda \nabla F_{\text{nom}} \\ (\alpha \nabla J_{\text{rbst}} - \lambda \nabla F_{\text{nom}})^T & -2\lambda(F_{\text{nom}} - f_0) - \gamma \end{bmatrix} \geq 0 \end{aligned} \quad (\text{B8}) \end{aligned}$$

Having obtained  $\lambda$ , the resulting optimal solution for the control increment is,

$$\tilde{v} = -(I - \lambda \nabla^2 F_{\text{nom}} + \alpha \nabla^2 J_{\text{rbst}})^{-1} (\alpha \nabla J_{\text{rbst}} - \lambda \nabla F_{\text{nom}}) \quad (\text{B9})$$

From [24], if there exists an increment  $\tilde{v}$  such that the constraint is a strict inequality, that is,  $F_{\text{quad}}(\tilde{v}) > f_0$ , then *strong duality* holds and the two objectives in (B7) and (B8) are equal, *i.e.*,

$$\tilde{v}^T (I + \alpha \nabla^2 J_{\text{rbst}}) \tilde{v} + 2\alpha \nabla J_{\text{rbst}}^T \tilde{v} = \gamma \quad (\text{B10})$$

Since  $F_{\text{nom}} > f_0$  and if the LMI in (B8) is positive definite, it follows that  $\gamma < -2\lambda(F_{\text{nom}} - f_0)$ . Thus  $\gamma$  is (theoretically) always negative which ensures that the quadratic approximation  $J_{\text{quad}}(\tilde{v})$  of  $J_{\text{rbst}}(v + \tilde{v})$  decreases. As we see in the numerical examples, the size of the decrease in  $J_{\text{rbst}}(v + \tilde{v})$  depends on the choice of the weighting parameter  $\alpha$  in the objective (B6). In addition, since we are roaming about near the top of the landscape where fidelity is very near to 1, the constraint that  $F_{\text{quad}}(\tilde{v}) \geq f_0$  is easily violated by very small amounts. These look large on the log-scale plots of fidelity error vs. iteration.

## Appendix C: Uncertainty Models

### 1. Linear time invariant noise

Although (30) captures *all* LTV filters, the overall character of the noise will dictate some specific forms. For example, suppose that it is only known that the noisy parameter has a limited bandwidth. The least complicated system which captures the bandwidth constraint only, is a first-order linear-time-invariant (LTI) system with time constant  $\beta$  (bandwidth is effectively  $1/\beta$ ) and whose input, sampled at  $T/M$ , is the stationary zero-mean white noise sequence  $\vec{w}$ ,  $\text{cov}(\vec{w}) = \delta_w^2 I_M$ . Then  $\theta_t, t = 1 : M$  is the output of the discrete-time *zero-order-hold* system with continuous-time transfer function  $1/(\beta s + 1)$ , *i.e.*,  $\Theta(z) = (1 - a)/(z - a)W(z)$  with  $a = \exp\{-\frac{T/M}{\beta}\}$ . It follows that the  $M \times M$  filter matrix  $\mathcal{K}$  in (30) is

$$\mathcal{K} = (1 - a) \begin{bmatrix} 1 & & & & \\ a & 1 & & & \\ & \vdots & \ddots & \ddots & \\ a^{M-1} & \dots & a & 1 & \end{bmatrix} \quad (\text{C1})$$

The discrete-time Fourier transform  $\Theta(\omega)$  of  $\theta_t, t = 1 : M$  is bounded by,

$$|\Theta(\omega)| \leq \delta \frac{1 - a}{\sqrt{2(1 - \cos(\omega T/M)) + a^2}} \quad (\text{C2})$$

### 2. PWC noise

A more extreme type of uncertain time-variation is where  $\theta_t$  is piece-wise-constant. Suppose  $\theta_t$  is constant but bounded over  $L$  uniform intervals  $\mathcal{T}_\ell$ , each of width  $T/L$  in  $[0, T]$ . Thus  $\theta_t$  changes abruptly  $L$  times (jumps) from a given underlying distribution. Suppose for each of the  $L$  intervals the uncertain parameter  $\theta_t, t \in \mathcal{T}_\ell$  is independently bounded by  $\|\theta_t, t \in \mathcal{T}_\ell\|_\infty \leq \delta_\infty$ . In other words, consider the *deterministic noise uncertainty set*,

$$\mathcal{H}_{\text{unc}} = \left\{ \tilde{H}_t = \theta_t B_t \left| \begin{array}{l} \theta_t = w_\ell, t \in \mathcal{T}_\ell, \ell = 1 : L \\ \|\theta_\ell\|_\infty \leq \delta_\ell \end{array} \right. \right\} \quad (\text{C3})$$

This type of uncertainty has an equivalent frequency domain spectrum. Since in each of the  $L$  time intervals the uncertain parameter varies independently, it can be considered as a time-sequence over  $[0, T]$  of uncertain amplitude  $\theta_\ell$  with a fixed duration  $T/L$ , *i.e.*, a pulse of known duration and uncertain magnitude bounded by  $\delta$ . For a deterministic uncertainty (C3), the magnitude of the Fourier transform  $\Theta(\omega)$  of such a sequence is bounded by the ‘‘sinc’’ function, *i.e.*, for each  $\ell = 1 : L$ ,

$$|\Theta_\ell(\omega)| \leq \delta \left( \frac{2\pi}{\omega_L} \right) \left| \text{sinc} \left( \frac{\omega\pi}{\omega_L} \right) \right|, \quad \omega_L = \frac{2\pi}{T/L} \quad (\text{C4})$$

As the number of intervals increase the spectral magnitude decreases while the bandwidth ( $\sim \omega_L$ ) increases, that is, the frequency spreads which potentially makes robustness more difficult to attain. The needed temporal behavior of  $\tilde{U}_t$  to overcome the frequency spread may be harder to realize under control limitations. The corresponding vector of the time-averaged Hamiltonian is,

$$\vec{G}_{\text{avg}} = \mathcal{A}S\vec{w} \quad \left\{ \begin{array}{l} \mathcal{A} = [\vec{\mathcal{A}}_1 \ \dots \ \vec{\mathcal{A}}_M] \\ S = \text{blk\_diag} [\mathbb{1}_{M/L} \ \dots \ \mathbb{1}_{M/L}] \\ \mathcal{A}_\ell = (1/M) \sum_{t \in \mathcal{T}_\ell} \tilde{U}_t^\dagger B_t \tilde{U}_t \end{array} \right. \quad (\text{C5})$$

where  $\mathbb{1}_{M/L}$  is an  $M/L$  vector of ones,  $\mathcal{A}$  is  $n^2 \times M$ ,  $S$  is  $M \times L$ , and  $\|\vec{w}\|_\infty \leq \delta$ . As a consequence, the robustness measure is the induced matrix norm,

$$J_{\text{rbst}} = \delta \|\mathcal{A}S\|_\infty \quad (\text{C6})$$

In effect, each of the piece-wise-constant uncertain parameters is reflected by a corresponding time-averaged Hamiltonian over each interval  $\mathcal{T}_\ell$  resulting in a collection of uncertain constant bounded parameters each of which is held fixed over some time intervals. For a probabilistic uncertainty where in

each of the  $L$  intervals  $\theta_t$  is zero-mean with covariance  $\delta^2 I_L$ , the corresponding robustness measure becomes,

$$J_{\text{rbst}} = \delta \|\mathcal{A}S\|_{\text{fro}} \quad (\text{C7})$$

### 3. Robustness measure as filter function

The robustness measure derived from the averaging approach is equivalent in at least one instance to a *filter function* measure as described in [8–16]. As an illustration, assume that the interaction Hamiltonian (6) is  $G(t) = \theta(t)A(t)$  with  $A(t) = \bar{U}(t)^\dagger B(t)\bar{U}(t)$ , where  $B(t)$  is known and where  $\theta(t)$  is a zero-mean wide-sense stationary random process with autocorrelation function,  $s(\tau) = \mathbf{E}\{\theta(t)\theta(t+\tau)\}$ . Clearly  $G(t)$  and the time-averaged Hamiltonian  $\langle G \rangle = (1/T)\int_0^T G(t)dt$  are both zero mean. Using the Frobenius norm to reflect the size of  $\langle G \rangle$ , let the robustness measure be the variance, *i.e.*,  $J_{\text{rbst}} = \mathbf{E}\|T\langle G \rangle\|_{\text{fro}}^2$  where expectation is with respect to the noise  $\theta(t)$ . The result is,

$$J_{\text{rbst}} = \int_{t=0}^T \int_{t'=0}^T s(t-t')c(t,t')dt'dt \quad (\text{C8})$$

$$c(t,t') = \mathbf{tr}(\bar{U}(t-t')^\dagger B(t)\bar{U}(t-t')B(t'))$$

Replace  $s(t-t')$  above by using the inverse Fourier transform  $s(\tau) = (1/2\pi)\int_{-\infty}^{\infty} S(\omega)e^{i\omega\tau}d\omega$  where  $S(\omega)$  is the associated power spectral density of the noise. This gives,

$$J_{\text{rbst}} = \int_{-\infty}^{\infty} \mathcal{A}(\omega)S(\omega)d\omega \quad (\text{C9})$$

with,

$$\mathcal{A}(\omega) = \frac{1}{2\pi} \int_{t=0}^T \int_{t'=0}^T e^{i\omega(t-t')} c(t,t')dt'dt \quad (\text{C10})$$

If in (C8), the known part of the uncertain perturbation is  $B(t) = B$ , a constant, then  $c(t,t') = c(t-t') = c(t'-t)$  which gives,

$$\mathcal{A}(\omega) = \frac{1}{\pi} \int_0^T (T-\tau)e^{i\omega\tau}c(\tau)d\tau \quad (\text{C11})$$

$$c(\tau) = \mathbf{tr}(\bar{U}(\tau)^\dagger B\bar{U}(\tau)B)$$

Sometimes  $S(\omega)$  can be measured, and even then, it can be approximated by (C2) and/or (C4). The frequency domain actuator dynamics error (C18) is also a candidate.

### 4. Additive control noise

Suppose that each of the  $m$  controls  $v_{jt}, j = 1 : m$  are affected by *additive noise*  $\{\theta_{jt}, t = 1 : M\}$ . As a result,  $v_{jt} = (\bar{v}_{jt} + \theta_{jt})H_c^j$  where  $\bar{v}_{jt}, j = 1 : m$ , the disturbance-free controls, serve as the design variables. As an illustration, suppose that the additive noise in control  $j$ , denoted by the  $M$ -vector  $\vec{\theta}_j$ , is the output of a filter  $\mathcal{K}_j$  as in (29)-(30) with  $\vec{w}_j$  being a zero-mean sequence with  $\text{cov}(\vec{w}_j) = \delta_w^2 I_M$ . This

is the same “model” of uncertainty as given by (34) except here we replace the time-varying  $B_{\ell t}$  with the constant control Hamiltonians  $H_c^j$ . The additive control noise Hamiltonian uncertainty set is,

$$\mathcal{H}_{\text{unc}} = \left\{ \begin{array}{l} \tilde{H}_t = \sum_{j=1}^m \theta_{jt} H_c^j, \left| \begin{array}{l} \vec{\theta}_j = \mathcal{K}_j \vec{w}_j, \vec{w}_j \text{ zero-mean} \\ \text{cov}(\vec{w}_j) = \delta_w^2 I_M \end{array} \right. \end{array} \right\} \quad (\text{C12})$$

Following the same procedure to arrive at (34), the robustness measure for this model of additive control noise is,

$$J_{\text{rbst}} = \sum_{j=1}^m \delta_j \|\mathcal{A}_j S_j\|_{\text{fro}} \quad \left\{ \begin{array}{l} \mathcal{A}_j = [\vec{A}_{j1} \ \cdots \ \vec{A}_{jM}] \\ \mathcal{A}_{jt} = \bar{U}_t^\dagger B_{jt} \bar{U}_t \\ S_j = \mathcal{K}_j / \|\mathcal{K}_j\|_{\text{fro}} \end{array} \right. \quad (\text{C13})$$

where each  $\mathcal{A}_j$  is  $n^2 \times M$ . Here we assumed that the noise affecting each control is independently drawn from different independent distributions each with its own spectrum (via  $\vec{\theta}_j = \mathcal{K}_j \vec{w}_j$ ). Though there are too many variations to delineate, such as noise drawn independently with the same spectrum, *e.g.*,  $\vec{\theta}_j = \mathcal{K}_j \vec{w}_j$ , or combinations thereof, the procedure to arrive at the appropriate robustness measure is the same. Moreover, the form of the robustness measure in all these cases will conform to the generic representation given by (11).

### 5. Multiplicative control noise

Suppose each of the  $m$  controls  $v_{jt}, j = 1 : m$  is affected by a time-varying *multiplicative noise* function  $\theta_{jt}$  such that  $v_{jt} = (1 + \theta_{jt})\bar{v}_{jt}H_c^j$  where, as previously described,  $\bar{v}_{jt}, j = 1 : m$  are the disturbance-free controls. As in the additive noise example, assume that for each control the noise is drawn independently from the same distribution. The associated Hamiltonian uncertainty set is almost identical to (C12) except for the dependence on the control:

$$\mathcal{H}_{\text{unc}} = \left\{ \begin{array}{l} \tilde{H}_t = \sum_{j=1}^m \theta_{jt} \bar{v}_{jt} H_c^j, \left| \begin{array}{l} \vec{\theta} = \mathcal{K} \vec{w}, \vec{w} \text{ zero-mean} \\ \text{cov}(\vec{w}) = \delta_w^2 I_{mM} \end{array} \right. \end{array} \right\} \quad (\text{C14})$$

Following the procedure to obtain (C13),

$$J_{\text{rbst}} = \sum_{j=1}^m \delta_j \|\mathcal{A}_j S_j\|_{\text{fro}} \quad \left\{ \begin{array}{l} \mathcal{A}_j = [\vec{A}_{j1} \ \cdots \ \vec{A}_{jM}] \\ \mathcal{A}_{jt} = \bar{v}_{jt} \bar{U}_t^\dagger B_{jt} \bar{U}_t \\ S_j = \mathcal{K}_j / \|\mathcal{K}_j\|_{\text{fro}} \end{array} \right. \quad (\text{C15})$$

The only difference between this measure and (C13) is that each disturbance-free control weighs the control Hamiltonians.



## 6. Uncertain actuator dynamics

Though not strictly noise, uncertain actuator (control generator) dynamics can appear in the form of a multiplicative control perturbation. Suppose the actuator dynamics are well modeled as an LTI system such that each of the  $m$  control commands  $\bar{v}_{tj}$  are effected by similar dynamics, *i.e.*,

$$v_{tj} = D_j(z)\bar{v}_{tj}, \quad j = 1 : m, \quad t = 1 : M \quad (\text{C16})$$

where  $D_j(z)$  is a rational transfer function in the unit delay operator  $z^{-1}$  corresponding to the sampling rate  $T/M$ . Assume that  $D_j(z)$  is in the uncertainty set,

$$\mathcal{D}(\Delta) = \left\{ D(z) = (1 + \Delta(z)Q(z))\bar{D}(z) \mid \begin{array}{l} \|\Delta\|_{\mathbf{H}_\infty} \leq \delta \\ \|Q\|_{\mathbf{H}_\infty} = 1 \end{array} \right\} \quad (\text{C17})$$

The transfer function  $\bar{D}(z)$  is the perturbation-free LTI model of the actuator dynamics,  $Q(z)$  is a normalized weighting factor, and  $\Delta(z)$  is a completely uncertain transfer function bounded in  $\mathbf{H}_\infty$  norm by  $\delta$ , the maximum magnitude of the frequency response. This set characterizes a standard transfer function with a bounded multiplicative model-error [29]. The equivalent frequency domain constraint is,

$$|D(i\omega)/\bar{D}(i\omega) - 1| \leq \delta|Q(i\omega)| \quad (\text{C18})$$

Since  $Q(z)$  is normalized, the left hand side can never exceed  $\delta$  over all frequencies.

The nominal and error Hamiltonians associated with this class of uncertainty are,

$$\begin{aligned} \bar{H}_t &= \sum_{j=1}^m (\bar{D}(z)\bar{v}_{tj})H_j \\ \tilde{H}_t &= \sum_{j=1}^m \theta_{tj}H_j \\ \theta_{tj} &= \Delta_j(z)Q(z)\bar{D}(z)\bar{v}_{tj} \end{aligned} \quad (\text{C19})$$

The time-averaged Hamiltonian (8) is then,

$$G_{\text{avg}} = \sum_{j=1}^m \frac{1}{M} \sum_{t=1}^M \theta_{tj} \bar{U}_t^\dagger H_j \bar{U}_t \quad (\text{C20})$$

For each  $j = 1 : m$ , write the  $M \times 1$  vector with elements  $\theta_{tj}, t = 1 : M$  as,

$$\text{vec}(\theta_j) = \mathcal{T}(\Delta_j(z))\mathcal{T}(Q(z)\bar{D}(z))\text{vec}(\bar{v}) \quad (\text{C21})$$

where  $\mathcal{T}(P(z))$  is a lower-triangular Toeplitz matrix whose first column is the impulse response of the LTI system  $P(z)$ . Since  $\|\Delta_j\|_{\mathbf{H}_\infty} \leq \delta$  implies that  $\|\mathcal{T}(\Delta_j(z))\|_2 \leq \delta$  [31], the robustness measure is similar to the form of (C15), namely,

$$\begin{aligned} J_{\text{rbst}} &= \delta \sum_{j=1}^m \|\mathcal{A}_j\|_2 S_j \\ \mathcal{A}_j &= \begin{bmatrix} \bar{A}_{1j} & \cdots & \bar{A}_{Mj} \end{bmatrix}, \quad A_{tj} = \bar{U}_t^\dagger H_j \bar{U}_t \\ S_j &= \|\mathcal{K}\text{vec}(\bar{v}_j)\|_2, \quad \mathcal{K} = \mathcal{T}(Q(z)\bar{D}(z)) \end{aligned} \quad (\text{C22})$$

## 7. Uncertain cross-couplings

An interesting class of closed systems with multiple errors, which has similarities to an *open* system, is one where the perturbations are caused by unwanted cross-coupling interactions amongst parallel channels. To illustrate this, consider two channels operating at the same time. With respective dimensions  $n_1$  and  $n_2$ , the system Hamiltonian is,

$$\begin{aligned} H_t &= \bar{H}_t + \tilde{H}_t \\ \bar{H}_t &= \bar{H}_t^{(1)} \otimes I_{n_2} + I_{n_1} \otimes \bar{H}_t^{(2)} \\ \tilde{H}_t &= \tilde{H}_t^{(1)} \otimes I_{n_2} + I_{n_1} \otimes \tilde{H}_t^{(2)} + \tilde{H}_t^{\text{int}} \end{aligned} \quad (\text{C23})$$

with uncertainty sets,

$$\begin{aligned} \tilde{H}_t^{(i)} &\in \mathcal{H}_{\text{unc}}^{(i)}, \quad i = 1, 2 \\ \tilde{H}_t^{\text{int}} &\in \mathcal{H}_{\text{unc}}^{\text{int}} \end{aligned} \quad (\text{C24})$$

The total system nominal unitary is the tensor product of each unperturbed channel:  $\bar{U}_t = \bar{U}_t^{(1)} \otimes \bar{U}_t^{(2)}$ . Consequently, the associated time-averaged Hamiltonian is,

$$\begin{aligned} G_{\text{avg}} &= G_{\text{avg}}^{(1)} \otimes I_{n_2} + I_{n_1} \otimes G_{\text{avg}}^{(2)} + G_{\text{avg}}^{\text{int}} \\ G_{\text{avg}}^{(i)} &= \frac{1}{M} \sum_{t=1}^M (\bar{U}_t^{(i)})^\dagger \tilde{H}_t^{(i)} \bar{U}_t^{(i)}, \quad i = 1, 2 \\ G_{\text{avg}}^{\text{int}} &= \frac{1}{M} \sum_{t=1}^M (\bar{U}_t^{(1)} \otimes \bar{U}_t^{(2)})^\dagger \tilde{H}_t^{\text{int}} (\bar{U}_t^{(1)} \otimes \bar{U}_t^{(2)}) \end{aligned} \quad (\text{C25})$$

In general each channel is attempting to make a different unitary. In this example there are two, denoted by  $W_i, i = 1, 2$ . Thus the nominal fidelity is the product of each as if they are independent,  $F_{\text{nom}} = F_{\text{nom}}^{(1)} F_{\text{nom}}^{(2)}$ , or equivalently,

$$F_{\text{nom}} = \left| \text{tr}(W^\dagger \bar{U}_N / n_1 n_2) \right|^2 \begin{cases} W = W_1 \otimes W_2 \\ \bar{U}_N = \bar{U}_N^{(1)} \otimes \bar{U}_N^{(2)} \end{cases} \quad (\text{C26})$$

There is some flexibility in the choice of the robustness measure. Consider, for example, the worst-case over the time-averaged Hamiltonians:

$$J_{\text{rbst}} = \max \left\{ \|G_{\text{avg}}^{\text{int}}\|, \|G_{\text{avg}}^{(1)}\|, \|G_{\text{avg}}^{(2)}\| \right\} \quad (\text{C27})$$

The norms in the regulation term  $J_{\text{rbst}}$  follow from the specific character of the uncertainty sets. This format is easily extended to more channels.

## 8. Open Systems

The robustness measures for two representative models of uncertain open systems are described: bipartite and Lindblad. These are both presented in the continuous-time framework.

### a. Bipartite

Consider a bipartite quantum system evolving over the time interval  $t \in [0, T]$  with “system” dimension  $n_S$  and “bath” dimension  $n_B$ . The continuous-time  $n = n_S n_B$  dimensional system-bath unitary  $U(t)$  is obtained from,

$$\begin{aligned} i\dot{U}(t) &= H(t)U(t) \\ H(t) &= H_S(t) \otimes I_{n_B} + I_{n_S} \otimes H_B(t) + H_{SB}(t) \end{aligned} \quad (\text{C28})$$

where  $H_S(t)$  is uncertainty-free and control dependent, and where  $H_B(t), H_{SB}(t)$  are uncertain with isolated unitaries,

$$i\dot{U}_S(t) = H_S(t)U_S(t), \quad i\dot{U}_B(t) = H_B(t)U_B(t) \quad (\text{C29})$$

For a “system” unitary target  $W_S$ , we use the fidelity as defined in [22],

$$F = \|\Gamma/n\|_{\text{nuc}}^2 \begin{cases} \Gamma = \sum_{i=1}^{n_S} V_{[ii]}, \\ V = (W_S \otimes I_{n_B})^\dagger U(T) \end{cases} \quad (\text{C30})$$

where  $\|\cdot\|_{\text{nuc}}$  is the nuclear-norm (sum of singular values), and where  $\{V_{[ii]}, i = 1 : n_S\}$  are the block-diagonal  $n_B \times n_B$  submatrices of the unitary  $V$ . (For a closed-system (no bath), this fidelity reduces to the standard  $F = |\text{tr}(W_S^\dagger U_S(T)/n_S)|^2$ ). In this case it is convenient to define the interaction unitary as,

$$R(t) = (U_S(t) \otimes U_B(t))^\dagger U(t) \quad (\text{C31})$$

Although in many instances the bath self-dynamics weakly interacts with the system, *e.g.*, the Hamiltonian  $H_B(t)$  is slowly varying over the operational time, here (C31) is appropriate with  $R(t)$  evolving from,

$$\begin{aligned} i\dot{R}(t) &= G(t)R(t) \\ G(t) &= (U_S(t) \otimes U_B(t))^\dagger H_{SB}(t)(U_S(t) \otimes U_B(t)) \end{aligned} \quad (\text{C32})$$

Suppose the time-averaged Hamiltonian  $\langle G \rangle \approx 0$  and the nominal fidelity  $F_{\text{nom}} = |\text{tr}(W_S^\dagger U_S(T)/n_S)|^2 \approx 1$ . Then  $R(T) \approx I$  and  $V \approx W_S^\dagger U_S(T) \otimes U_B(T) \approx I_{n_S} \otimes U_B(T)$ . Under these conditions the fidelity (C30) is  $F \approx 1$ . It follows from these assumptions that the appropriate robustness measure is,

$$J_{\text{rbst}} = \max_{H_B, H_{SB} \in \mathcal{H}_{\text{unc}}} \left\| \frac{1}{T} \int_0^T G(t) dt \right\| \quad (\text{C33})$$

The specific norm depends on the characteristics of  $\mathcal{H}_{\text{unc}}$ .

### b. Lindblad

A basic Lindblad master equation describes non-unitary evolution of an  $n \times n$  density matrix  $\rho(t), t \in [0, T]$  by,

$$\begin{aligned} \dot{\rho} &= -i[\bar{H}(t), \rho] + \mathcal{L}(\rho, \theta), \quad \rho(0) = \rho_0 \\ \mathcal{L}(\rho, \vec{\theta}) &= \sum_{k=1}^K \theta_k \left( 2L_k \rho L_k^\dagger - (L_k L_k^\dagger \rho + \rho L_k L_k^\dagger) \right) \end{aligned} \quad (\text{C34})$$

where  $\bar{H}(t)$  is the nominal (uncertainty-free) Hamiltonian as defined in (1). Here the Lindblad term  $\mathcal{L}(\rho, \vec{\theta})$  is an uncertainty model with known operations  $L_k \in \mathbb{C}^{n \times n}, k = 1 : K$ , where  $\vec{\theta}$  is a  $K \times 1$  vector of uncertain coefficients  $\theta_k$  bounded in norm by  $\|\vec{\theta}\| \leq \delta$ .

To reconfigure the Lindblad system (C34) into our standard multicriterion optimization form (11), lift the density to the vector  $x(t) = \vec{\rho}(t) \in \mathbb{C}^{n^2}$ . Then (C34) becomes,

$$\begin{aligned} \dot{x} &= -iA(t)x + B(\vec{\theta})x, \quad x(0) = \vec{\rho}_0 \\ A(t) &= I_n \otimes \bar{H}(t) - \bar{H}(t)^* \otimes I_n \\ B(\vec{\theta}) &= \sum_{k=1}^K \theta_k B_k \\ B_k &= 2(L_k^* \otimes L_k) - (I_n \otimes L_k^\dagger L_k + (L_k^\dagger L_k)^T \otimes I_n) \end{aligned} \quad (\text{C35})$$

Note that the nominal (uncertainty-free) system,

$$\dot{\bar{x}} = -iA(t)\bar{x}, \quad \bar{x}(0) = \vec{\rho}_0 \quad (\text{C36})$$

has as solution,

$$\bar{x}(t) = \bar{V}(t)\vec{\rho}_0 \begin{cases} \dot{\bar{V}}(t) = \bar{U}(t)^* \otimes \bar{U}(t) \\ \dot{\bar{U}}(t) = -i\bar{H}(t)\bar{U}(t), \quad \bar{U}(0) = I_n \end{cases} \quad (\text{C37})$$

Let the lifted state  $x(t) = \bar{V}(t)R(t)\vec{\rho}_0$  where  $R(t)$ , the lifted  $n^2 \times n^2$  interaction unitary, evolves from,

$$\begin{aligned} \dot{R}(t) &= G(t, \vec{\theta})R(t), \quad R(0) = I_{n^2} \\ G(t, \vec{\theta}) &= \bar{V}(t)^\dagger B(\vec{\theta})\bar{V}(t) = \sum_{k=1}^K \theta_k \bar{V}(t)^\dagger B_k \bar{V}(t) \end{aligned} \quad (\text{C38})$$

Here  $G(t, \vec{\theta})$  is the lifted interaction Hamiltonian. A target unitary  $W$  is achieved at the final time  $T$  if the density matrix  $\rho(T) \approx W\rho_0 W^\dagger$  for all  $\rho_0$ , or in terms of the lifted state,  $x(T) \approx \text{vec}(W\rho_0 W^\dagger) = (W^* \otimes W)\vec{\rho}_0$ . Following (A12) together with (C38) gives the corresponding distance and fidelity measures,

$$\begin{aligned} \mathcal{E} &= \min_{|\phi|=1} \|\bar{V}(T)R(T) - \phi(W^* \otimes W)\|_{\text{fro}}^2 \\ &= 2n^2(1 - \mathcal{F}) \\ \mathcal{F} &= \left| \text{tr}((W^* \otimes W)^\dagger (\bar{U}(T)^* \otimes \bar{U}(T))R(T)) / n^2 \right| \end{aligned} \quad (\text{C39})$$

Because we have lifted  $\rho$  to  $\vec{\rho}$ , thereby inflating the dimension from  $n$  to  $n^2$ , the fidelity here,  $\mathcal{F}$ , is not squared as in (A12). To see why this is appropriate, if  $R(T) \approx I_{n^2}$ , then  $\mathcal{F} \approx F_{\text{nom}} = |\text{tr}(W^\dagger \bar{U}(T)/n)|^2$  as usual.

Since the uncertainty is bounded,  $\|\vec{\theta}\| \leq \delta$ , it follows that the robustness measure follows from the corresponding induced matrix norm of the time-averaged interaction Hamiltonian,

$$J_{\text{rbst}} = \max_{\|\vec{\theta}\| \leq \delta} \|T\vec{G}_{\text{avg}}(\vec{\theta})\| = \delta \|\mathcal{A}\| \quad (\text{C40})$$

with

$$\begin{aligned} \mathcal{A} &= [\vec{\Gamma}_1 \ \dots \ \vec{\Gamma}_k] \in \mathbb{C}^{n^4 \times K} \\ \Gamma_k &= \int_0^T \bar{V}(t)^\dagger B_k \bar{V}(t) dt \end{aligned} \quad (\text{C41})$$

## Appendix D: Numerical examples

### 1. Multiplicative control noise

Continuing with the single qubit system, let  $\theta_t$  denote multiplicative control noise, that is,

$$H_t = (1 + \theta_t)v_t\sigma_x + \sigma_z \quad (\text{D1})$$

Here we set  $N = 10$  PWC control pulses, again  $M = 50$  noise samples, and the identity target. The multiplicative noise is uniformly random in  $\pm 0.05$  with *five* changes over the time interval as described by the ‘‘sinc’’ spectrum (C4). Thus the noise level randomly changes *twice* during every control pulse window. The resulting robustness measure is given by (C15) for  $\ell = 1 : 5$  with  $\mathcal{A}_\ell = (1/M) \sum_{t \in \mathcal{T}_\ell} v_t \bar{U}_t^\dagger \sigma_x \bar{U}_t$ . For this case of a scalar control, except for the inclusion of the control pulse magnitude, the robustness measure reduces to the form (C6).

Figure 3(a)-(c) displays the simulation results. These clearly follow the pattern of Figure 3(a)-(f) with some notable differences. First, the uncertainty improvement at the extremes of the noise level range  $\pm 0.05$  is, on average, one order of magnitude, unlike the additive noise results which is nearly two orders of magnitude. Secondly, there is no discernible control pattern for the robust set of pulses as previously seen in the additive noise case. These observations may vary from system to system. However, it is striking that the fidelity error and robustness measure plots per iteration follow the expected behavior as predicted to be available by the control landscape topology analysis.

### 2. Drift and multiplicative uncertainty

An illustrative single-qubit example of a system with two uncertainties is,

$$H_t = (1 + \theta_z)\sigma_z + (1 + \theta_{x,t})v_t\sigma_x \quad (\text{D2})$$

where  $\theta_z$  is an uncertain constant parameter (a bias) and  $\theta_{x,t}$  is a time-varying multiplicative control noise. The correspond-

ing uncertainty set is,

$$\mathcal{H}_{\text{unc}} = \left\{ \begin{array}{l} \tilde{H}_t = \theta_z \sigma_z + \theta_{x,t} v_t \sigma_x \\ \theta_z = \delta_z w_z \\ \vec{\theta}_x = \delta_x \mathcal{K}_x \vec{w}_x \\ |w_z| \leq 1, \|\vec{w}_x\|_\infty \leq 1 \end{array} \right. \quad (\text{D3})$$

where  $\mathcal{K}_x$  is a Toeplitz matrix representation of the noise dynamics as described in §V F. Taking the robustness measure as the sum of the robustness measures for each uncertainty type yields,

$$J_{\text{rbst}} = \|\mathcal{A}S\|_\infty \left\{ \begin{array}{l} \mathcal{A} = [\mathcal{A}_z \ \mathcal{A}_x] \\ \mathcal{A}_z = \vec{A}_z, \mathcal{A}_z = (1/M) \sum_{t=1}^M \bar{U}_t^\dagger \sigma_z \bar{U}_t \\ \mathcal{A}_x = [\vec{A}_{x,1} \ \dots \ \vec{A}_{x,M}] \\ \mathcal{A}_{x,t} = v_t \bar{U}_t^\dagger \sigma_x \bar{U}_t / M, t = 1 : M \\ S = \begin{bmatrix} \delta_z & 0 \\ 0 & \delta_x \mathcal{K}_x \end{bmatrix} \end{array} \right. \quad (\text{D4})$$

Figure 4(a)-(c) shows results of the two-stage optimization to make the identity gate with  $N = 5$  PWC control pulses,  $M = 10$  averaging samples, a constant drift uncertainty range of  $\delta_z = 0.05$ , and a multiplicative noise with magnitude  $\delta_x = 0.01$  drawn from a uniform distribution with the ‘‘sinc’’ spectrum (C4) with  $L = 2$ , *i.e.*, two-pulses of width  $1/L$ . Equivalently, the noise dynamics are modeled by the matrix  $\mathcal{K}_x = \text{blk\_diag}(\mathbb{1}_{M/2}, \mathbb{1}_{M/2})$ . Thus  $S$  is an  $M + 1 \times 3$  matrix.

As seen in Figure 4(a), we increased the fidelity threshold  $f_0$  two times during the iterations which allowed for a continuous improvement in robustness.

Figure 4(b) shows approximately an order of magnitude increase (red), on average, as compared to the noise-free response (blue). The data for these plots is from random samples  $\theta^i = Sw^i, i = 1, \dots, 100$  with  $w^i \in \mathbb{R}^{M+1}$  uniformly random in  $\pm 1$ . The final robust control pulses shown in Figure 4(c) reveal an interesting symmetric pattern. This suggests a possible deeper connection between this class of uncertainties and robustness.

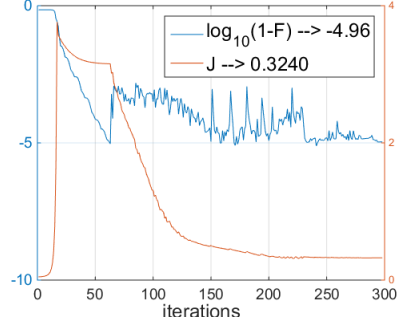
### 3. Amplitude and phase control noise

Consider a single-qubit system having amplitude and phase control *e.g.*, laser control. A simplified Hamiltonian model is,

$$H_t = (\Omega_t/2) (\sigma_x \cos \phi_t + \sigma_y \sin \phi_t) \left\{ \begin{array}{l} \Omega_t = (1 + \tilde{\Omega}_t) \bar{\Omega}_t \\ \phi_t = \bar{\phi}_t + \tilde{\phi}_t \end{array} \right. \quad (\text{D5})$$

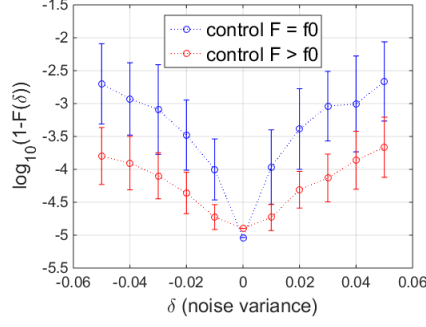
where  $(\bar{\Omega}_t, \bar{\phi}_t)$  are the known control commands and where  $(\tilde{\Omega}_t, \tilde{\phi}_t)$  are time-varying perturbations, respectively, multiplicative in control and additive in phase. An approximate

Infidelity &amp; robustness vs. iterations



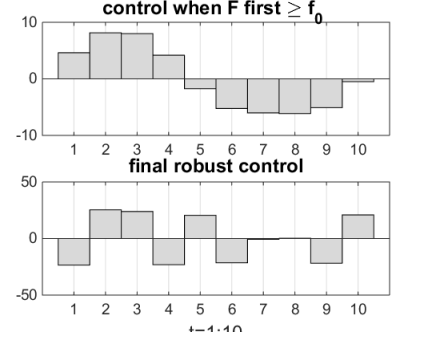
(a)

Evaluation of infidelity vs. uncertainty



(b)

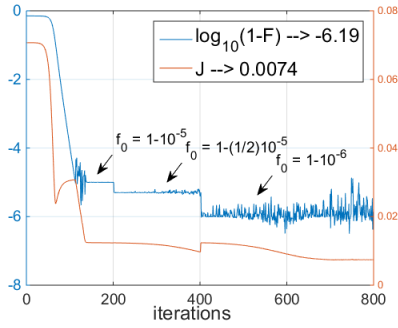
Control pulses: nominal vs. optimal



(c)

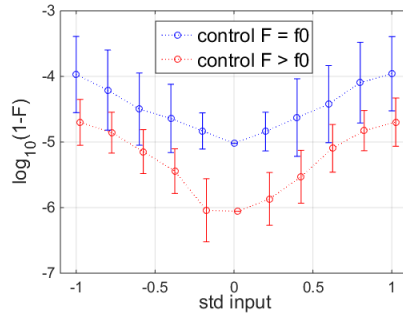
FIG. 3. Uncertain time-varying multiplicative control parameter  $H_t = (1 + \theta_t)v_t\sigma_x + \sigma_z$ .

Infidelity &amp; robustness vs. iterations



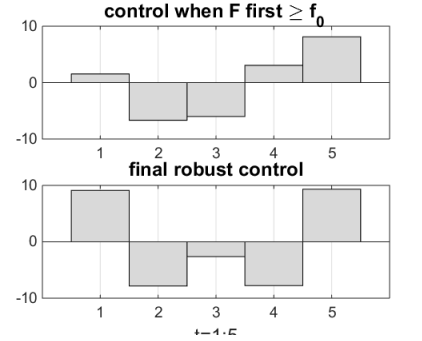
(a)

Evaluation of infidelity vs. uncertainty



(b)

Control pulses: nominal vs. optimal



(c)

FIG. 4. Two uncertainties  $H_t = (1 + \theta_{x,t})v_t\sigma_x + (1 + \theta_z)\sigma_z$ .

Hamiltonian to first-order in these perturbations is,

$$H_t \approx \bar{H}_t + \tilde{H}_t \begin{cases} \bar{H}_t = \bar{v}_{x,t}\sigma_x + \bar{v}_{y,t}\sigma_y \\ \tilde{H}_t = \tilde{\Omega}_t\bar{H}_t + \tilde{\phi}_t\bar{H}_t^\phi \\ \bar{H}_t^\phi = \bar{v}_{x,t}\sigma_y - \bar{v}_{y,t}\sigma_x \end{cases} \quad (\text{D6})$$

with  $\bar{H}_t$  the nominal (noise-free) Hamiltonian, a linear function of the ideal (noise-free) controls  $\bar{v}_{x,t} = (\bar{\Omega}_t/2) \cos \bar{\phi}_t$  and  $\bar{v}_{y,t} = (\bar{\Omega}_t/2) \sin \bar{\phi}_t$ . Use of this approximate model (D6) for control synthesis is not strictly necessary; it suffices here because the perturbations are small. The full model (D5) is used for the final analysis and validation. Note that both perturbations are effectively in the form of multiplicative noise as defined in (C14).

For this example, let both perturbations arise from the output of LTI filters driven by independent white noise, each drawn from a normal distribution with respective variances  $\delta_\Omega^2$  and  $\delta_\phi^2$ . As in (31), the LTI filter dynamics is contained in the Toeplitz matrices ( $\mathcal{K}_\Omega, \mathcal{K}_\phi$ ) where each first column is the impulse response. The resulting robustness measure is of the

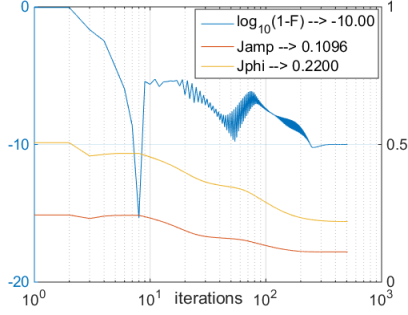
same form as (D4), effectively the sum of two measures, *i.e.*,

$$J_{\text{rbst}} = \|\mathcal{A}S\|_{\text{fro}} \begin{cases} \mathcal{A} = [\mathcal{A}_\Omega \ \mathcal{A}_\phi] \\ \mathcal{A}_\Omega = [\vec{A}_{\Omega,1} \ \dots \ \vec{A}_{\Omega,M}] \\ \mathcal{A}_{\Omega,t} = \vec{U}_t^\dagger \bar{H}_t \vec{U}_t / M, \ t = 1 : M \\ \mathcal{A}_\phi = [\vec{A}_{\phi,1} \ \dots \ \vec{A}_{\phi,M}] \\ \mathcal{A}_{\phi,t} = \vec{U}_t^\dagger \bar{H}_t^\phi \vec{U}_t / M, \ t = 1 : M \\ S = \begin{bmatrix} \delta_\Omega \mathcal{K}_\Omega & 0 \\ 0 & \delta_\phi \mathcal{K}_\phi \end{bmatrix} \end{cases} \quad (\text{D7})$$

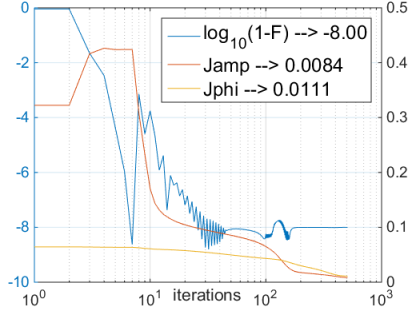
Figure 5 shows results of the two-stage optimization to make the Hadamard gate with  $N = 20$  PWC control pulses for each of the two controls over a time interval of  $T = 10$  time units. The number of averaging samples is  $M = 200$  and the threshold to switch from Stage-1 to Stage-2 is set very high at  $f_0 = 1 - 10^{-10}$ .

In the example shown in Figure 5(a)-(c) the perturbation noise dynamics affecting amplitude and phase are identical low-pass filters with bandwidth at 1/2 the Nyquist frequency ( $\omega_{\text{nyq}} = \pi/(T/M)$ ).

Infidelity &amp; robustness vs. iterations

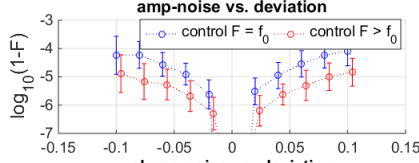


(a)

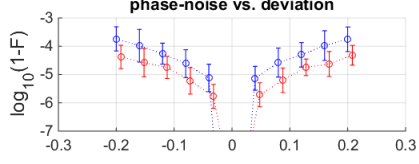


(d)

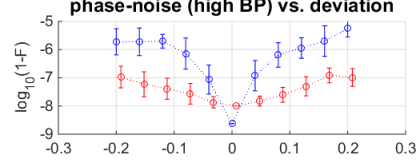
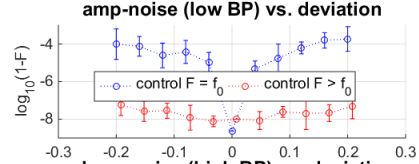
Evaluation of infidelity vs. uncertainty



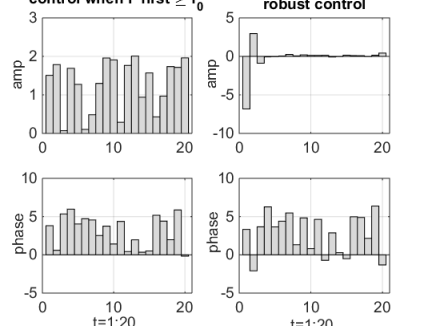
(b)



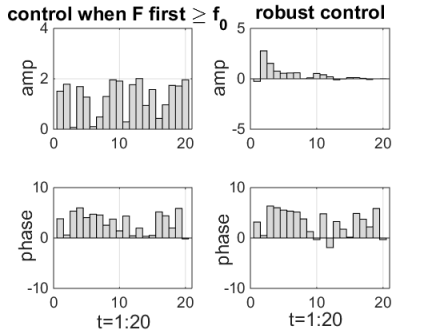
(e)



Control pulses: nominal vs. optimal



(c)



(f)

FIG. 5. **Two uncertainties.** (a)-(c) **System (D5)**: amplitude and phase control are simultaneously affected by noise from two *identical* low pass noise filters with bandwidth at  $1/2$  the Nyquist frequency, where each filter is driven by independent white noise. (d)-(f) **System (D5)**: amplitude and phase control affected simultaneously by two *different* bandpass noise filters: low bandpass for amplitude, high bandpass for phase. (see Figure 6).

In the example shown in Figure 5(d)-(f) the noise filters are not identical, both amplitude and phase noise are each independently generated from bandpass digital Chebyshev filters whose filter frequency magnitudes and (normalized) impulse responses are shown in Figure 6. Each filter has 0.5 decibels of peak-to-peak ripple in the passband with the amplitude noise passband at the low end of the Nyquist frequency, namely  $[0.01, 0.02]\omega_{\text{nyq}}$ , whereas the phase noise passband is at the high end at  $[0.5, 0.6]\omega_{\text{nyq}}$ .

All the iterations in column 1 of Figure 5 show the (expected) rapid Stage-1 optimization to make the noise-free system fidelity reach the selected very high threshold. Then the Stage-2 optimization turns on whose goal is to hold the threshold while reducing robustness. The fidelity oscillations occur while the two robustness measures decrease until an equilibrium or stopping criterion are reached.

Column 2 of Figure 5 shows the post-optimization evaluation on the full system. The worst-case fidelities with the bandpass filter noise are considerably improved in Figure 5(d)-(f) over those of the low pass noise analysis seen in Figure 5(a)-(c). This behavior is perhaps expected since the noise frequencies are more concentrated via the narrow frequency ranges of the bandpass noise filters.

As we have repeatedly remarked, upon viewing the control pulses in column 3 of Figure 5, no discernible reason is easily forthcoming to account for the achieved significant robust-

ness, except that it was requested of the available null space control resource at the top of the landscape.

#### 4. Uncertain cross-couplings

Following (C23), an example (discrete-time) Hamiltonian of a two qubit system with uncertain local parameters in each system and an uncertain cross coupling term is,

$$H_t = (v_{1t}\sigma_x + \theta_1\sigma_z) \otimes I_2 + I_2 \otimes (v_{2t}\sigma_x + \theta_2\sigma_z) + \theta_{12}(\sigma_x^{\otimes 2} + \sigma_y^{\otimes 2} + \sigma_z^{\otimes 2}) \quad (\text{D8})$$

with constant uncertain parameters all in the same range  $(\theta_1, \theta_2, \theta_{12}) \in [-0.005, 0.005]$ . The final time is  $T = 10$  with  $N = 20$  PWC pulses per control and  $M = 40$  uniform samples for simulation. The unitary targets for system 1 and 2 are, respectively, the Hadamard and Identity gates, that is,  $W_1 = (\sigma_x + \sigma_z)/\sqrt{2}$  and  $W_2 = I_2$ . The initial system 1 and 2 controls,  $v_{1t}$  and  $v_{2t}$ , are selected to make these gates robust locally, *i.e.*, assuming no cross-coupling ( $\theta_{12} = 0$ ), and uncertainty only in  $(\theta_1, \theta_2)$ . In other words, these initial controls are robust to the independent variations of  $(\theta_1, \theta_2)$  with no knowledge of cross-coupling uncertainty.

The iteration plots in Figure 7(a) start with each control be-



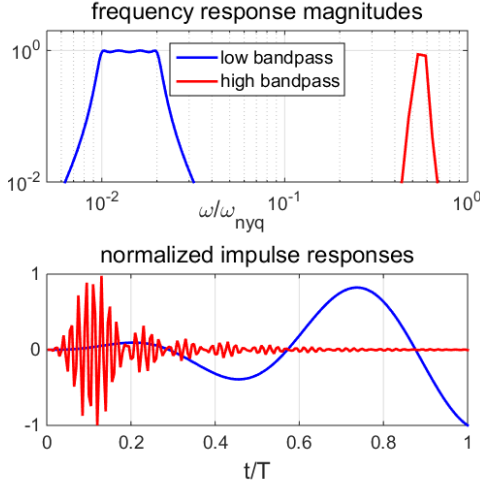
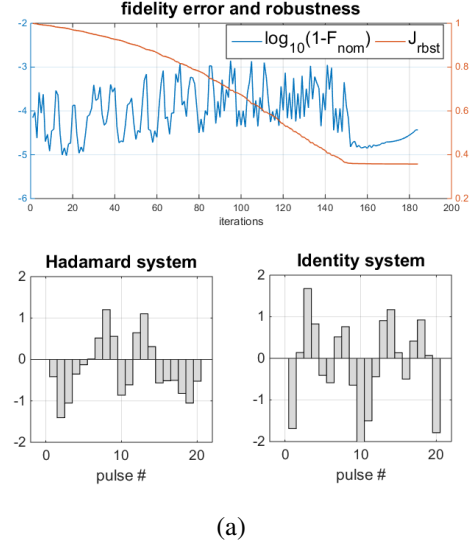


FIG. 6. **Chebyshev BandPass Filters** The upper plots shows the magnitudes of the low and high BP frequency response magnitudes. The lower plot shows the normalized impulse responses: slow variations for the low frequency BP and rapid oscillations for the high frequency BP.

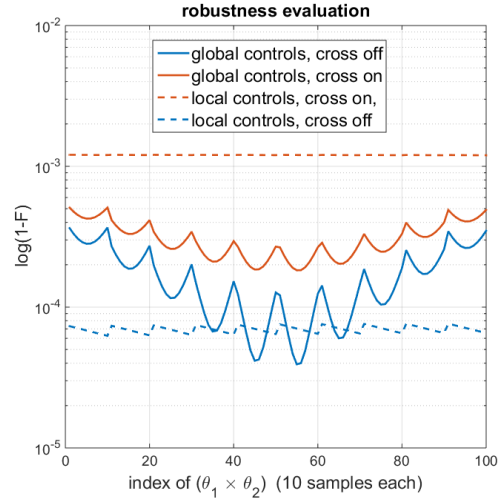
ing robust to its own local uncertainty with no knowledge of the cross-coupling uncertainty. We see again that fidelity remains at a high fidelity level-set while the time-averaged regulation term  $J_{rbst}$  (C27) falls until it can no longer be changed.

The results of these individual and independent optimal controls are shown in Figure 7(b) with respect to both the local uncertainty which is very low (dashed blue plot) whereas considerable degradation occurs when the cross-coupling is included (dashed red plot) even though it is a small amount.

By contrast the global robust controls, which account for both local and cross-coupling uncertainties, show only a slight increase in fidelity error robustness due to the coupling uncertainty as seen in Figure 7(b) (solid red plots) vs. no coupling (solid blue plots). With coupling (solid red plot) there is significant robustness improvement compared to the local robust controls with coupling present.



(a)



(b)

FIG. 7. **Cross coupling uncertainty.** (a)Top. Fidelity error ( $1 - F_{nom}$ ) and robustness measure ( $J_{rbst}$ ) vs. iterations. Initial controls are robust to local uncertainty only. (a)Bottom. Pulse magnitudes of robust control to simultaneous local system and cross-coupling uncertainty. (b) Fidelity error vs. uncertain parameters with independent local (dashed) & global (solid) robust controls.